Mohamed Khider University of Biskra
Faculty of Science and Technology
Department of Electrical Engineering

MASTER'S THESIS

Science and Technology
Electrotechnics
Electrical Networks

Réf : Enter the document reference

Presented and defended by:

AICHE Zakaria & CHETTHOUNA Takki eddine

On: June 2025

OPTIMAL REACTIVE POWER DISPATCH CONSIDERING VARIOUS UNCERTAINTIES IN POWER SYSTEM

Jury :

SALHI SOUHEIL	MCB	University of Biskra	President
SALHI AHMED	Pr	University of Biskra	Supervisor
NAIMI DJEMAI	Pr	University of Biskra	Examiner

CLASS OF 2024 / 2025


بسم الله الرحمن الرحيم

Abstract

Optimal Reactive Power Dispatch (ORPD) is essential for ensuring economic, secure, and voltage-stable operation of power systems. It represents a complex nonlinear optimization problem aimed at determining the optimal control settings while satisfying system constraints. To address this challenge, the Hippopotamus Optimization Algorithm (HO), a recent metaheuristic, was employed to minimize key performance indicators such as active power losses (Ploss), total voltage deviation (TVD), and the voltage stability index (VSI). The algorithm was tested on IEEE 30-bus and IEEE 57-bus systems in deterministic conditions, where it demonstrated superior performance compared to other optimization techniques. Additionally, a probabilistic scenario-based uncertainty modeling approach was applied to reflect real-world fluctuations in load demand and wind power generation. This uncertainty analysis was performed on the IEEE 30-bus system, focusing on minimizing Ploss under stochastic conditions. The results confirmed the robustness and effectiveness of the HO algorithm in both deterministic and uncertain environments.

Key words: Optimal reactive power dispatch (ORPD), Total transmission active losses (Ploss), Total voltage deviation (TVD), Voltage stability index (VSI),Hippopotamus optimization algorithm (HO).

ملخص :

يعد التوزيع الأمثل للاستطاعة الرجعية(ORPD)مسألة ضرورية لضمان التشغيل الاقتصادي الآمن والمستقر من حيث الجهد لأنظمة القدرة الكهربائية. حيث يمثل مسألة تحسين غير خطية ومعقدة تهدف إلى تحديد الإعدادات المثلى لعناصر التحكم مع احترام قيود النظام. لمعالجة هذا التحدي، تم توظيف خوارزمية فرس النهر للأمثلة (HO)، وهي خوارزمية ميتااستكشافية حديثة، بهدف تقليل مؤشرات الأداء الرئيسية مثل الفقد في الاستطاعة الفعالة (Ploss)، والانحراف الكلي للجهد (TVD) ، ومؤشر استقرار الجهد.(VSI) وقد تم اختبار هذه الخوارزمية على نظامي IEEE 30-bus و IEEE 57-bus في ظروف حتمية، حيث أظهرت أداءً متفوقًا مقارنةً بتقنيات الأمثلة الأخرى. بالإضافة إلى ذلك، تم اعتماد نهج نمذجة قائم على السيناريوهات الاحتمالية لتمثيل التقلبات الواقعية في الطلب على الأحمال وتوليد الطاقة من الرياح. وقد تم إجراء هذا التحليل في ظل عدم اليقين على نظام-30 IEEE bus، مع التركيز على تقليل الاستطاعة الفعالة (Ploss) في ظروف عشوائية. وأكدت النتائج فعالية وقوة خوارزمية HOفي بيئات التشغيل الحتمية وغير الحتمية على حد سواء.

الكلمات المفتاحية:توزيع الأمثل للاستطاعة الرجعية(ORPD)، الفقد في الاستطاعة الفعالة (Ploss)، الانحراف الكلي للجهد(TVD) ، مؤشر استقرار الجهد(VSI) ، خوارزمية فرس النهر للأمثلة .(HO)

Résumé :

La répartition optimale de la puissance réactive (ORPD) est essentielle pour assurer un fonctionnement économique, sûr et stable des réseaux électriques. Il s'agit d'un problème d'optimisation non linéaire complexe visant à déterminer les paramètres de contrôle optimaux tout en satisfaisant les contraintes du système. Pour relever ce défi, l'algorithme d'optimisation Hippopotamus (HO), une métaheuristique récente, a été utilisé pour minimiser les indicateurs de performance clés tels que les pertes de puissance active (Ploss), la déviation totale de la tension (TVD) et l'indice de stabilité de la tension (VSI). L'algorithme a été testé sur des systèmes IEEE 30-bus et IEEE 57-bus dans des conditions déterministes, où il a démontré des performances supérieures à celles d'autres techniques d'optimisation. En outre, une approche de modélisation probabiliste de l'incertitude basée sur des scénarios a été appliquée pour refléter les fluctuations réelles de la demande de charge et de la production d'énergie éolienne. Cette analyse d'incertitude a été réalisée sur le système IEEE à 30 bus, en se concentrant sur la minimisation du Ploss dans des conditions stochastiques. Les résultats ont confirmé la robustesse et l'efficacité de l'algorithme HO dans des environnements déterministes et incertains.

Mots clés : Répartition optimale de la puissance réactive (ORPD), pertes actives totales de transmission (Ploss), déviation totale de la tension (TVD), indice de stabilité de la tension (VSI), algorithme d'optimisation Hippopotamus (HO).

Acknowledgement

We would first like to thank Allah for granting us the health, strength, and patience needed to complete this work.

We express our sincere gratitude to our supervisor, Pr. SALHI Ahmed, for his valuable guidance, availability, and constructive feedback throughout this project.

Our thanks also go to the jury members for accepting to evaluate this humble work.

Finally, we wish to express our deep appreciation to all the professors who have supported and taught us from the first year to the final year at Mohamed Khider University of Biskra.

2025

Dedication

I dedicate this work to the two pillars of my life, To my dear parents, whose love, sacrifices, and unwavering support have shaped who I am today. Your prayers have been my light in times of doubt, and your guidance has been my compass throughout this journey.

To my beloved sisters, thank you for your constant encouragement and belief in me. Your presence has been a source of motivation and comfort.

To my dear brother, thank you for always being there with your support, kindness, and quiet strength. You've been a true source of encouragement.

And to my friends, who stood by my side, shared my challenges, and celebrated my successes this journey wouldn't have been the same without you.

I dedicate this humble work to all of you, with deep love and sincere gratitude.

ZAKARIA

Dedication

First and foremost, I thank Allah, the Most Merciful, the source of all wisdom and strength, for guiding me throughout this journey and granting me the patience and perseverance to complete this work.

I dedicate this memoir to my beloved parents, whose unwavering love, sacrifices, and endless support have been my foundation. Your belief in me has carried me through every challenge.

To my dear friends, thank you for standing by me, encouraging me, and sharing in both the difficult moments and the joyful ones. Your companionship has made this journey more meaningful.

With deep gratitude and love,

This work is for all of you.

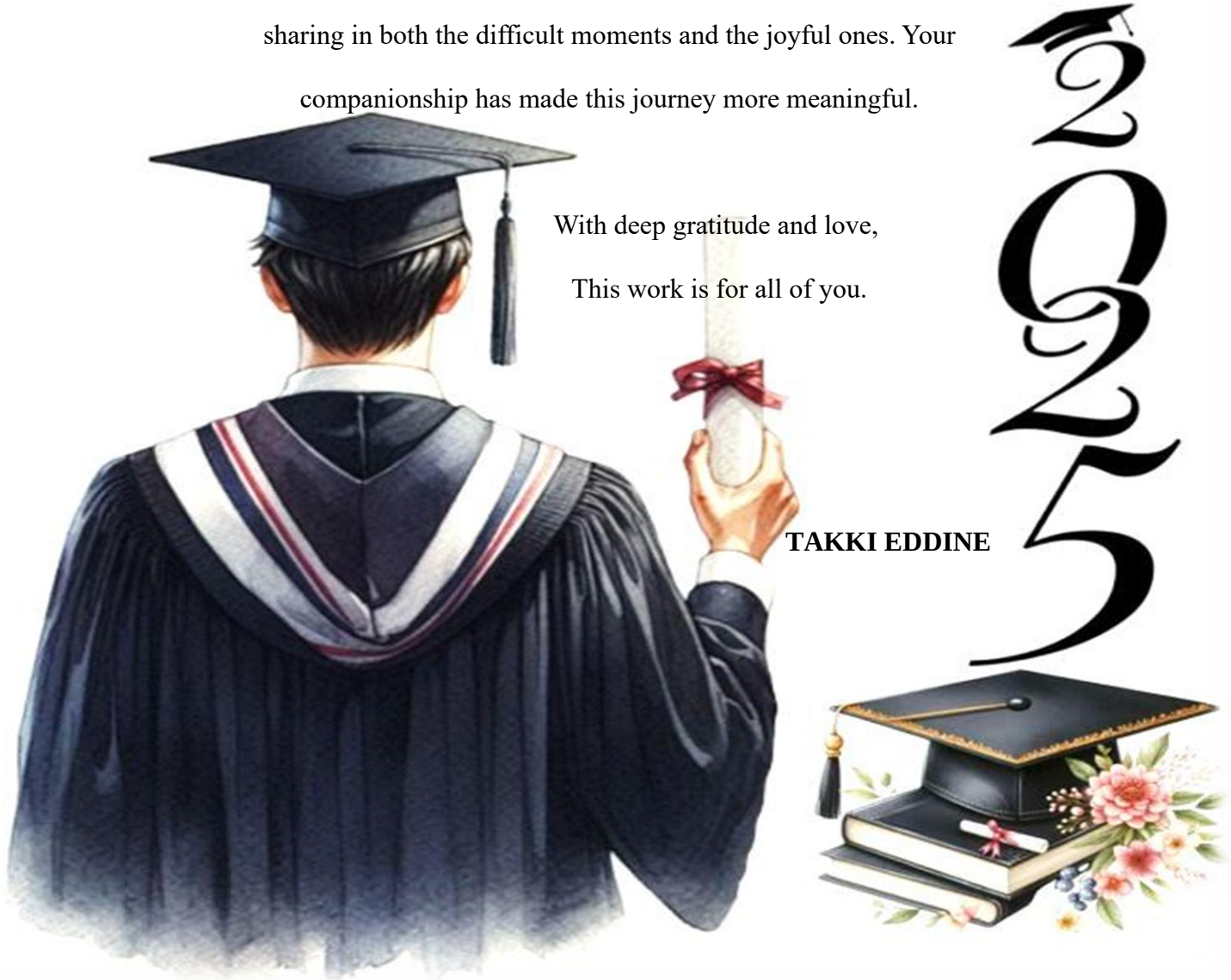

TAKKI EDDINE

Table of contents

Chapter 2 : Optimal power flow

Chapter 3 : The hippopotamus optimization algorithm

Chapter 4: Simulation results and analysis

List of Figures

List of Tables

General introduction

General introduction

The modern electrical power network is undergoing significant transformation due to the massive integration of renewable energy sources, growing demand, and increasing requirements for reliability, stability, and energy efficiency. In this context, power systems are becoming increasingly complex, dynamic, and exposed to various uncertainties, particularly those related to load variability, wind power generation, and real-world operating conditions. If not properly accounted for, these uncertainties can compromise service quality, increase energy losses, and negatively impact system stability.

Reactive power requirements vary continuously with changes in load and system configuration, leading to corresponding voltage fluctuations. Any alteration in network topology or power demand can affect voltage levels across the system, When the circulation of reactive power is not properly coordinated, it can lead to undesirable voltage deviations, degrading power quality and threatening voltage stability, particularly in heavily loaded or weakly meshed networks.

To address these challenges, the Optimal Reactive Power Dispatch (ORPD) problem has emerged as a key operational strategy. which seeks to determine the optimal control variables including generator voltages, transformer tap settings, and reactive power compensation devices. By strategically dispatching reactive power, the ORPD problem aims to improve voltage profiles, enhance voltage stability, and reduce overall system losses. In particular, controlling reactive power helps maintain the modulus of bus voltages |V| within desired limits, which is essential for ensuring high-quality and stable power delivery.

Traditionally, ORPD has been solved using deterministic approaches such as nonlinear programming and Newton-Raphson-based methods. However, due to the nonlinear, non-convex, and often discontinuous nature of the objective functions and constraints, these conventional methods face several limitations, especially when dealing with large-scale systems or uncertainties. As a result, nature-inspired metaheuristic algorithms have gained increasing attention in recent years.

In this work, we focus on solving the ORPD problem considering various uncertainties, by employing a recent nature-inspired metaheuristic technique named Hippopotamus Optimization Algorithm (HO). The newly developped approach is applied

under both deterministic and probabilistic conditions. In the deterministic case, the performance of HO is benchmarked against several well-established algorithms using IEEE standard test systems. In contrast, under uncertain conditions, we focus on evaluating the performance of HO alone, using a scenario-based probabilistic modeling approach to represent uncertainties in both load demand and wind power generation.

The primary objectives of this study:

Improve power system performance by minimizing active power losses (Ploss), reducing total voltage deviation (TVD) and enhancing the voltage stability index (VSI) using the new optimization method (HO) under deterministic conditions.

Comparining simulation results of the proposed approach to those of other well-known metaheuristic algorithms.

Modeling system uncertainties through probabilistic scenario-based approaches to assess their impact on system performances by minimizing active power losses (Ploss).

This thesis is structured as follows:

Chapter 1 introduces the fundamentals of electric power systems and power flow analysis.

Chapter 2 details the formulation of the ORPD problem as sub-problem of Optimal Power Flow (OPF), including objective functions, constraints, solution methods, and the modeling of uncertainties using probabilistic approaches.

Chapter 3 presents the Hippopotamus Optimization Algorithm (HO), covering its biological inspiration, mathematical modeling and optimization procedure steps.

Chapter 4 presents and discusses the ORPD simulation results obtained for the IEEE 30-bus and IEEE 57-bus test systems under deterministic conditions. While the ORPD simulation for probalistic conditions are reserved to IEEE 30-bus test system for both wind and load under uncertainty conditions.

Chapter 1:

Power flow

1.1 Introduction :

Today, electricity plays a very important role in our daily lives, and every country considers this energy as an essential means for its social and economic development. Even the slightest electrical problem significantly impacts the continuity of economic activities ,In This chapter we presents the problems of power flow, describing the numerical methods used for the study of load distribution in an electrical network. Also we provides an overview of the topology of electrical networks. It focuses on the structure of transmission and distribution networks.

1.2 Overview of Electrical Network Systems :

Electrical networks are complex systems that transport electricity from generation sources to consumers through various components like transmission lines and substations. It consists of power lines operated at different voltage levels, connected with substations. Electric substations allow the distribution and transmission of electricity from one voltage level to another using transformers. An electrical grid must also ensure the dynamic management of the entire production - transport - consumption system, implementing adjustments aimed at ensuring the stability of the whole. [1]

The electrical network system can be divided into three main functions As shown in Figure (1.1):

- production
- transport
- distribution

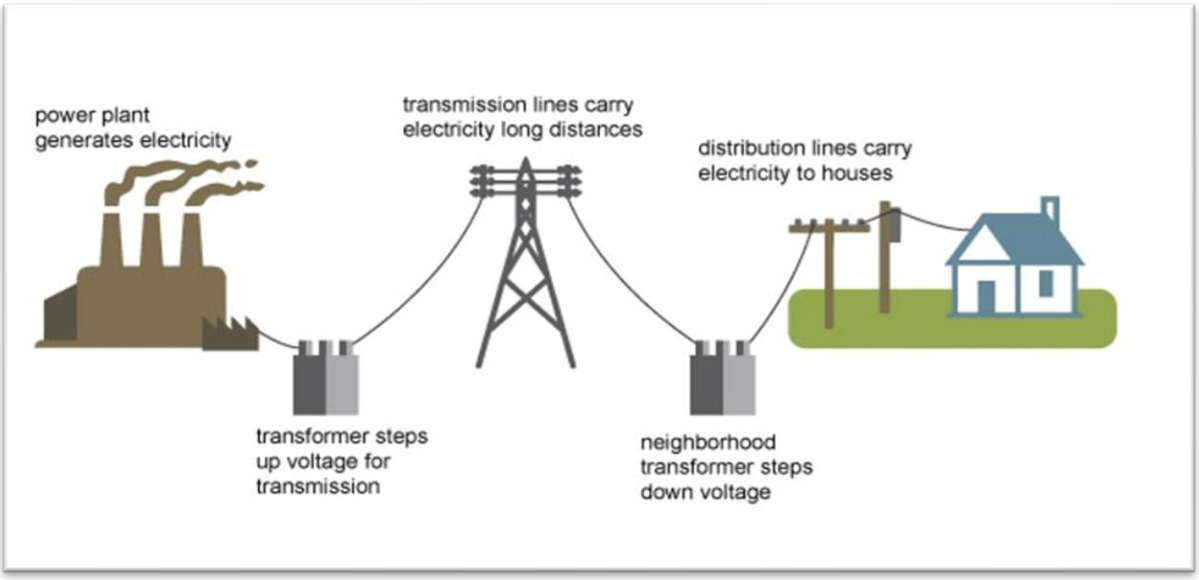

Figure 1. 1 : Simplified electrical network [2]

1.2.1 Production :

Today's electricity network is complicated, interconnected, and constantly evolving in scale and structure. A significant portion of electricity comes from conventional power sources, such as thermal, hydroelectric, and nuclear plants. Another share is generated by non-conventional renewable sources, often referred to as green energy due to its lower pollutant emissions.[3]

Electrical energy is generated in power stations using generators at voltages ≤ 20,000 volts. Typically, these stations are situated far from consumption centers due to technical and environmental considerations, including emissions.

As electric current flows through transmission lines, energy is lost due to the resistance of the conductors.[4]

1.2.2 Transport :

Once electricity is generated, it is transported to consumption points through power lines. High-voltage electricity is carried by overhead transmission lines supported by tall steel towers.

The electricity then arrives at a substation (containing transformers and distribution equipment), where the voltage is stepped down from high to medium levels before being fed into the distribution network.

However, some power stations bypass transmission lines entirely. In such cases, the electricity is converted to medium voltage immediately and sent straight to the distribution network. This approach depends on factors like the power plant's location and the amount of electricity being transmitted. [4]

1.2.3 Distribution :

The distribution system is in charge of delivering power from substations to final consumers, including residences, workplaces, and manufacturing facilities. The high voltage from the transmission network is now lowered to safer levels that are appropriate for consumer usage through the use of transformers. In order to provide consumers with dependable and secure power transmission, the distribution network consists of transformers, switchgear, and overhead and subterranean wires. The distribution system aims to reduce service disruptions and maintain a steady voltage.

1.3 Modelling of electrical network components :

In power flow, we don't need to represent every single aspect of the electrical network Instead, we focus on the critical components that impact how the system functions. These include generators, electrical loads, transmission lines, transformers, and static compensators. The model should contain enough detail to assist regulate the network and assure its stable operation.

1.3.1 Generators :

The "synchronous generator," also known as a three-phase alternating current generator, is regarded as the most crucial component of the electrical grid. At the node to which it is linked, a steady voltage source injects an active power Pg and a reactive power Qg. For the generator's output to stay consistent and within the system's production limits, turbine control must be used to adjust its active power. To maintain a steady voltage at the alternator terminals, on the other hand, the reactive power fluctuates between the two limit values, minimum (Qgmin) and maximum (Qgmax) [5] .

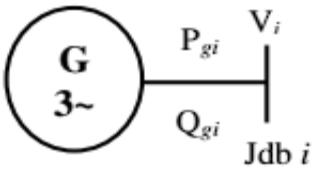

Figure 1. 2 : Model of generator [6].

1.3.2 Transmission lines :

The transmission line is generally represented by its equivalent π model, as shown in Figure (1.3) This model is widely used to simplify the analysis of transmission systems. The parameters associated with this model are as follows : [7]

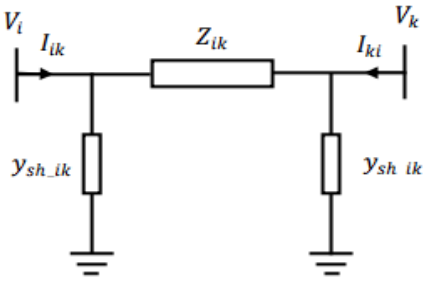

Figure 1. 3 : Modèle en π d'une ligne de transport [6].

The series impedance Z_{ik} of the line:

$$Z_{ik} = R_{ik} + jX_{ik} \tag{1.1}$$

R_{ik}: a resistance in series

X_{ik} : inductive reactance

The shunt admittance $y_{\mathrm{sh}_{ik}}$ on each side of the line:

$$y_{\mathrm{sh}_{ik}} = \frac{G_{ik} + jB_{ik}}{2} \tag{1.2}$$

G_{ik} : is the insulation conductance of the line between the two busbars i and k

B_{ik} : is the capacitive susceptance of the line between the two busbars i and k.

1.3.3 Power transformer :

The power transformer is commonly modeled as an asymmetrical equivalent circuit Π, as illustrated in this Figure **:**

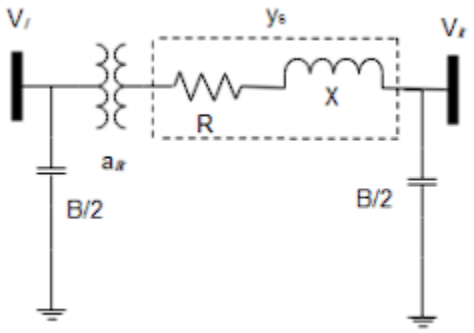

Figure 1. 4 : π Model of an Ideal Transformer [6].

This model includes key parameters used for analysis, such as impedance and admittance values. Power transformers play a crucial role in adjusting voltage levels and ensuring efficient power transfer across different parts of the electrical network. [6]

1.3.4 Electrical loads :

Loads are typically substations that supply distribution networks and are statically modeled as negative power injections at busbars. The load is connected to the network through a load tap changer transformer that maintains a constant voltage level. As a result, the active and reactive powers of the load can be represented by constant values, denoted as P_d and Q_d [4] .

1.3.5 Shunt elements:

Shunt elements are generally used to compensate reactive power and regulate voltage. Common devices include synchronous machines, capacitor banks, fixed reactors, and static VAR compensators (SVC). They are modeled either through equivalent admittance or by injecting reactive power into the system. [8]

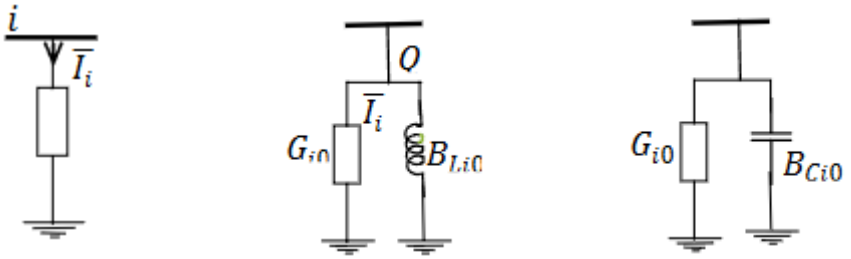

a) Symbols b) inductive element c) capacitive element

Figure 1. 5 : Model of shunt elements [8].

$$Y_{i0} = G_{i0} + jB_{i0} \tag{1.3}$$

G_{i0} is the conductance (active power losses, usually small), and B_{i0} is the susceptance (reactive power exchange positive for capacitive, negative for inductive).

1.4 Classification of variables in power flow equations:

1.4.1 disturbance variables :

These are uncontrolled variables that represent the active and reactive powers demanded by the loads. They are considered as unknown or unpredictable inputs to the system. The disturbance vector is given by:

$$P = [P_{D1} \quad P_{D2} \quad P_{D3} \quad \ldots . P_{Dn}]^T \tag{1.4}$$

$$Q = [Q_{D1} \quad Q_{D2} \quad Q_{D3} \quad \ldots Q_{Dn}]^T \tag{1.5}$$

1.4.2 State variables :

The voltage magnitudes and phase angles are key variables that define the operating state of the electrical power system. Specifically, these include $|V_1|, |V_2|, |\delta_1|, |\delta_2|$, which together form the state vector X. This vector provides essential information for analyzing and monitoring the overall behavior and stability of the system.

$$X = (V_1 \quad V_2 \quad \delta_1 \quad \delta_2) \tag{1.6}$$

1.4.3 Control variables :

Control variables typically include the active powers generated and the generator terminal voltages The key control variables are: P_{G1}, P_{G2}, V_{G1}, V_{G2} . These help in optimizing power flow and managing the system's dynamic response. [9]

$$\mathbf{U} = (P_{G1} \quad P_{G2} \quad V_{G1} \quad V_{G2}) \tag{1.7}$$

1.5 Classifications of busses :

In power system modeling, busbars are typically classified into three main types depending on which variables are specified:

1. Reference (Slack) Bus
2. Load Bus (P–Q Bus)
3. Generator Bus (P–V Bus)

Generally, 80% to 90% of the buses in a system are load buses, about 1% are slack buses, and the rest are generator buses. For each bus, two variables are known, while the other two are determined through power flow calculations [10] .

1.5.1 Slack Bus (|V|, δ) :

The slack bus is the reference bus in a power system where the voltage magnitude $|V|$ and angle δ are specified. The generated active power P_g and reactive power Q_g are unknown and are calculated during the power flow process. This bus compensates for total system losses and imbalances, so it must be connected to a source capable of providing both real and reactive power. Choosing the right slack bus requires system-specific experience, as it can affect the stability of the solution.[10]

1.5.2 Load Bus (PQ Bus) :

A load bus is where the active power demand P_d and reactive power demand Q_d are specified. The voltage magnitude and angle are unknowns to be solved in power flow analysis. Even if a generator is present, any bus with defined complex power injection is typically treated as a load bus for modeling simplicity. [10]

1.5.3 Generation bus (PV Bus) :

At a voltage controlled (or PV) bus, the generated active power P_g and voltage magnitude$|V|$ are known. The reactive power Q_g and voltage angle are calculated during analysis, within predefined limits. These buses must include a reactive power control element like a generator or capacitor bank to regulate voltage effectively. [11]

Table 1. 1 : Types of buses in an electrical network.

Type of buses	Known variables	Unknown variables
Slack bus (reference)	$\boldsymbol{|V|, \delta}$	$\boldsymbol{P_g, Q_g}$
Load bus (PQ)	$\boldsymbol{Q_d, P_d}$	$\boldsymbol{|V|, \delta}$
Generation bus (PV)	$\boldsymbol{P_g, |V|}$	$\boldsymbol{Q_g, \delta}$

1.6 Power flow :

The power flow analysis is a very important an fodanmuntal tool in power system based on steady-state that used to ascertain the network's operating circumstances. At each bus, it determines the voltage magnitude V, voltage angle δ, active power P, reactive power Q, and power flows in the transmission lines. The dependable and effective functioning of electrical power systems depends on this information.

1.6.1 Objectives of Power Flow:

- Ensure the balance between the production and demand of electric energy.
- Avoid exceeding limit values (theoretical stability and proper duration of use).
- Maintain bus-bar voltages within theoretical limits.
- Increase the security of network operation through good power flow strategy before disturbances .

1.7 Power flow formulation :

In this subsection, we will construct the power flow equations in a structured manner using the admittance matrix Y_{bus} representation of the transmission network. The admittance matrix $Y_{bus}$is assumed to be known for the system under consideration. [12]

For a power system with N busbars, the system's nodal voltage equations are expressed by the matrix relationship : [13]

$$\begin{bmatrix} \bar{I}_1 \\ \bar{I}_2 \\ \vdots \\ \bar{I}_N \end{bmatrix} = \begin{bmatrix} \bar{Y}_{11} & \bar{Y}_{12} & \cdots & \bar{Y}_{1N} \\ \bar{Y}_{21} & \bar{Y}_{22} & \cdots & \bar{Y}_{2N} \\ \vdots & \vdots & \ddots & \vdots \\ \bar{Y}_{N1} & \bar{Y}_{N2} & \cdots & \bar{Y}_{NN} \end{bmatrix} \begin{bmatrix} \bar{V}_1 \\ \bar{V}_2 \\ \vdots \\ \bar{V}_N \end{bmatrix} \tag{1.8}$$

Or

$$I_{bus} = Y_{bus} V_{bus} \tag{1.9}$$

I_{bus} :is the vector of the complex currents injected into each busbar .

V_{bus} :is the vector of the complex voltages of each busbar .

Y_{bus} :is the nodal admittance matrix of the system.

The nodal admittance matrix is formed based on power system components such as transmission lines, transformers, capacitor banks, and reactors. Each component can connect between two buses I and m, or between a bus I and the reference bus. The matrix elements are calculated based on the admittances of these components using specific rules [12].

The diagonal element $\bar{Y}_{ii}$represents the total admittance of all components connected directly to busbar i.

$$\bar{Y}_{ii} = \sum_{\substack{m=0 \\ m \neq i}}^{N} \bar{y}_{im} \tag{1.10}$$

$\overline{Y}_{im}$ The off-diagonal element im ,is equal to the negative of the total admittance of all components connected between busbars i and m. N is the total number of buses.

$$\overline{Y}_{im} = -\sum_{m \neq i} \bar{y}_{im} \tag{1.11}$$

According to equation (1.8), the net current injected at a busbar i can be written as follows:

$$\bar{I}_i = \sum_{m=1}^{N} \bar{Y}_{im} \bar{V}_m, \quad i = 1,2, \ldots, N \tag{1.12}$$

The complex quantities $\bar{V}_m$ and Y_{im} are represented in polar or rectangular form as follows:

$$\bar{V}_m = V_m \cos\delta_m + jV_m \sin\delta_m = e_m + jf_m$$
$$\bar{Y}_{im} = Y_{im}\cos\theta_{im} + jY_{im}\sin\theta_{im} = G_{im} + jB_{im} \quad (1.13)$$

δ_m: Phase angle of the voltage at bus m .

θ_{im}: Phase (or argument) of the admittance matrix element .

e_m: Real part of the voltage $\bar{V}_m$.

f_m: Imaginary part of the voltage $\bar{V}_m$.

G_{im}: Real part (conductance) of the admittance $\bar{Y}_{im}$.

B_{im}: Imaginary part (susceptance) of the admittance $\bar{Y}_{im}$.

The expression for the apparent power Si injected into a busbar i is obtained by:

$$\bar{S}_i = P_i + jQ_i = \bar{V}_i \bar{I}_i^* = \bar{V}_i \sum_{m=1}^{N} \bar{Y}_{im}^* \bar{V}_m^*, \quad i = 1,2,\dots,N \quad (1.14)$$

By replacing (1.13) in (1.14),

we have:

$$P_i = \sum_{m=1}^{N} V_i V_m Y_{im} \cos(\delta_i - \delta_m - \theta_{im}) \qquad with\ i = 1 \dots N \quad (1.15)$$

$$Q_i = \sum_{m=1}^{N} V_i V_m Y_{im} \sin(\delta_i - \delta_m - \theta_{im}) \qquad with\ i = 1 \dots N \quad (1.16)$$

This set of 2 nonlinear equations represents the polar form of the power flow equations, describing the injections of active power P_i and reactive power Q_i at bus i, as given by the following expressions. [13]

$$P_i = P_{Gi} - P_{Di} \quad with \quad i = 1,2,\dots,N \quad (1.17)$$

$$Q_i = Q_{Gi} - Q_{Di} \quad with \quad i = 1,2,\dots,N \quad (1.18)$$

P_{Gi} Active power generated at bus i .

P_{Di}: Active power demanded (load) at bus i .

Q_{Gi}: Reactive power generated at bus i .

Q_{Di}: Reactive power demanded (load) at bus i .

Finally, the power balance equations are given in the following form:

$$P_{Gi} = P_{Di} + \sum_{m=1}^{N} V_i V_m Y_{im} \cos(\delta_i - \delta_m - \theta_{im}) \qquad with\ i = 1 \dots N \tag{1.19}$$

$$Q_{Gi} = Q_{Di} + \sum_{m=1}^{N} V_i V_m Y_{im} \sin(\delta_i - \delta_m - \theta_{im}) \qquad with\ i = 1 \dots N \tag{1.20}$$

1.8 Methods for Solving the Power Flow Problem :

1.8.1 Newton-Raphson :

The Newton–Raphson method for load flow analysis is considered more efficient and practical for large-scale power systems due to its quadratic convergence and greater stability in handling ill-conditioned problems. In any multi-bus network, the fundamental equation is expressed using the nodal admittance matrix form ,is gived by : [14]

$$I_i = \sum_{j=1}^{N} Y_{ij} V_j \tag{1.21}$$

I_i : is the current entering into bus i.

N : the total number of buses .

The power flow equations are often written in polar form since PV bus actual power and voltage magnitude are supplied in load flow issues.
The ith bus voltage and transfer admittance are often represented in polar coordinates as follows:

$$V_i = |V_i| \angle \delta_i = |V_i|(\cos\delta_i + j\sin\delta_i) = |V_i| e^{j\delta_i} \tag{1.22}$$

And

$$Y_{ij} = |Y_{ij}|(\cos\alpha_{ij} + j\sin\alpha_{ij}) = |Y_{ij}| e^{j\alpha_{ij}} \tag{1.23}$$

$|Y_{ij}|$:Magnitude of admittance between bus i and bus j .

α_{ij} :Phase angle of admittance between bus i and bus j .

Equation (1.21) in polar form we have :

$$I_i = \sum_{j=1}^{N} |Y_{ij}|\,|V_j| \angle \varphi_{ij} + \delta_j \tag{1.24}$$

The bus power at bus-i is given by:

$$P_i - jQ_i = V_i^* I_i = V_i^* \sum_{j=1}^{N} Y_{ij}\, V_j \tag{1.25}$$

Substitution of the polar forms of V_i and Y_{ij} in Equation . (1.25)

$$P_i - jQ_i = \sum_{j=1}^{N} |V_i|\,\big|V_j\big|\big|Y_{ij}\big| \mathrm{e}^{j(\varphi_{ij}+\delta_j-\delta_i)} \tag{1.26}$$

Since from trigonometry,

$$\mathrm{e}^{j(\varphi_{ij}+\delta_j-\delta_i)} = \cos(\varphi_{ij} + \delta_j - \delta_i) + j\sin(\varphi_{ij} + \delta_j - \delta_i) \tag{1.27}$$

Therefore, after separating the real and imaginary components, substituting Eq. (1.26) in Eq. (1.27) results in

$$P_i = \sum_{j=1}^{N} |V_i|\,\big|V_j\big|\big|Y_{ij}\big| \cos(\varphi_{ij} + \delta_j - \delta_i) \tag{1.28}$$

$$Q_i = -\sum_{j=1}^{N} |V_i|\,\big|V_j\big|\big|Y_{ij}\big| \sin(\varphi_{ij} + \delta_j - \delta_i) \tag{1.29}$$

For small variations of δ and $|V|$, a linear relationship is obtained by forming the partial differrential equations as follows: [14]

$$\Delta P_i = \sum_{j=1}^{NB} \frac{\partial P_i}{\partial \delta_j} \Delta\delta_j + \sum_{j=1}^{NB} \frac{\partial P_i}{\partial |V_j|} \Delta |V_j| \tag{1.30}$$

Equation (1.30) is valid for all type of buses excluding the slack bus. Also,

$$\Delta Q_i = \sum_{j=1}^{N} \frac{\partial Q_i}{\partial \delta_j} \Delta\delta_j + \sum_{j=1}^{N} \frac{\partial Q_i}{\partial |V_j|} \Delta |V_j| \tag{1.31}$$

For all non–voltage-controlled (PQ) buses, equation (1.31) applies. Therefore, in an N-bus system without voltage-controlled buses, the equations can be expressed as follows:

$$\begin{bmatrix} \Delta P_2^{(k)} \\ \vdots \\ \Delta P_N^{(k)} \\ \hline \Delta Q_2^{(k)} \\ \vdots \\ \Delta Q_N^{(k)} \end{bmatrix} = \begin{bmatrix} \frac{\partial P_2^{(k)}}{\partial \delta_2} & \cdots & \frac{\partial P_2^{(k)}}{\partial \delta_N} & \frac{\partial P_2^{(k)}}{\partial |V_2|} & \cdots & \frac{\partial P_2^{(k)}}{\partial |V_N|} \\ \vdots & & \vdots & \vdots & & \vdots \\ \frac{\partial P_N{}^{(k)}}{\partial \delta_2} & \cdots & \frac{\partial P_N^{(k)}}{\partial \delta_N} & \frac{\partial P_N^{(k)}}{\partial |V_2|} & \cdots & \frac{\partial P_N^{(k)}}{\partial |V_N|} \\ \frac{\partial Q_2^{(k)}}{\partial \delta_2} & \cdots & \frac{\partial Q_2^{(k)}}{\partial \delta_N} & \frac{\partial Q_2}{\partial |V_2|} & \cdots & \frac{\partial Q_2^{(k)}}{\partial |V_N|} \\ \vdots & & \vdots & \vdots & & \vdots \\ \frac{\partial Q_N{}^{(k)}}{\partial \delta_2} & \cdots & \frac{\partial Q_N^{(k)}}{\partial \delta_N} & \frac{\partial Q_N^{(k)}}{\partial |V_2|} & \cdots & \frac{\partial Q_N^{(k)}}{\partial |V_N|} \end{bmatrix} \begin{bmatrix} \Delta \delta_2^{(k)} \\ \vdots \\ \Delta \delta_N^{(k)} \\ \hline \Delta |V_2^{(k)}| \\ \vdots \\ \Delta |V_N^{(k)}| \end{bmatrix} \tag{1.32}$$

Again Eqs. (1.30) and (1.31) can be written as ;

$$\Delta P_i = \sum_{j=1}^{N} J_1 \, \Delta \delta_j + \sum_{j=1}^{N} J_2 \, \Delta |V|_j \tag{1.33}$$

$$\Delta Q_i = \sum_{j=1}^{N} J_3 \, \Delta \delta_j + \sum_{j=1}^{N} J_4 \, \Delta |V|_j \tag{1.34}$$

In matrix form, these equations can be represented as follows:

$$\begin{bmatrix} \Delta P \\ \Delta Q \end{bmatrix} = \begin{bmatrix} J_1 J_2 \\ J_3 J_4 \end{bmatrix} \begin{bmatrix} \Delta \delta \\ \Delta |V| \end{bmatrix} \tag{1.35}$$

Or, in abbreviated form:

$$\begin{bmatrix} \Delta P \\ \Delta Q \end{bmatrix} = [J] \begin{bmatrix} \Delta \delta \\ \Delta |V| \end{bmatrix} \tag{1.36}$$

The elements of the Jacobian matrix $[J]$ are derived from the partial derivatives of equations (1.28) and (1.29) with respect to $\Delta\delta$ and $\Delta|V|$, as shown below:

For quardrant [J1]:

Diagonal elements:

$$\frac{\partial P_i}{\partial \delta_i} = \sum_{\substack{j=1 \\ j \neq i}}^{N} |V_i||V_j||Y_{ij}| \sin(\varphi_{ij} + \delta_j - \delta_i) \tag{1.37}$$

Off − diagonal elements :

$$\frac{\partial P_i}{\partial \delta_j} = -|V_i||V_j||Y_{ij}| \sin(\varphi_{ij} + \delta_j - \delta_i); \quad i \neq j \tag{1.38}$$

For quardrant [J2]:

Diagonal elements:

$$\frac{\partial P_i}{\partial |V_i|} = 2|V_i||Y_{ii}|\cos\varphi_{ii} + \sum_{\substack{j=1 \\ j\neq i}}^{N} |V_j|\,|Y_{ij}|\cos(\varphi_{ik} + \delta_k - \delta_i) \tag{1.39}$$

Off − diagonal elements:

$$\frac{\partial P_i}{\partial |V_j|} = |V_i||Y_{ij}|\cos(\varphi_{ij} + \delta_j - \delta_i); \quad i \neq j \tag{1.40}$$

For quardrant [J3]:

Diagonal elements:

$$\frac{\partial Q_i}{\partial \delta_i} = \sum_{\substack{j=1 \\ j\neq i}}^{N} |V_i|\,|V_j||Y_{ij}|\cos(\varphi_{ij} + \delta_j - \delta_j) \tag{1.41}$$

Off − diagonal elements :

$$\frac{\partial Q_i}{\partial \delta_k} = -|V_i||V_j||Y_{ij}|\cos(\varphi_{ij} + \delta_j - \delta_i); \quad i \neq j \tag{1.42}$$

For quardrant [J4]:

Diagonal elements:

$$\frac{\partial Q_i}{\partial |V_i|} = -2|V_i||Y_{ii}|\sin\varphi_{ii} + \sum_{\substack{j=1 \\ j\neq i}}^{N} |V_j|\,|Y_{ij}|\sin(\varphi_{ij} + \delta_j - \delta_i) \tag{1.43}$$

Off − diagonal elements :

$$\frac{\partial Q_i}{\partial |V_j|} = -|V_i||Y_{ij}|\sin(\varphi_{ij} + \delta_j - \delta_i); \quad i \neq j \tag{1.44}$$

If the system has mmm voltage-controlled buses, then there are (N−1) buses with active power constraints and (N−1−m) buses with reactive power constraints. As a result,

the Jacobian matrix has dimensions of [2(N−1)−m]×[2(N−1)−m], with submatrices of the following order:

$$\begin{aligned} J_1 &\text{ is of the order of } && [N-1]\times[N-1], \\ J_2 &\text{ is the order of } && [N-1]\times[N-1-m], \\ J_3 &\text{ is of the order of } && [N-1-m]\times[N-1], \\ J_4 &\text{ is of the order of } && [N-1-m]\times[N-1-m]. \end{aligned}$$

Once the Jacobian elements are formulated, any one can develop the process of solving the load flow problem by Newton-Raphson method as follows: [15]

Step 1: Start by reading input data, forming the **Y-bus matrix**, and initializing voltages:

Load buses: $\left|V_i^{(0)}\right| = 1.0, \qquad \delta_i^{(0)} = 0.$

Voltage-regulated buses: $\delta_i^{(0)} = 0.$

Step 2: Calculate power mismatches for load buses:

$$\Delta P_i^{(k)} = P_{i,\text{scheduled}} - P_{i,\text{calculated}}^{(k)}. \tag{1.45}$$

$$\Delta Q_i^{(k)} = Q_{i,scheduled} - Q_{i,calculated}^{(k)}. \tag{1.46}$$

Step 3: For **voltage-controlled buses**, compute only $\Delta P_i^{(k)}$ (no reactive power mismatch).

Step 4: Check convergence $\left|\Delta P_i^{(k)}\right|$and $\left|\Delta Q_i^{(k)}\right|$for all the buses whether they are less than the specified accuracy or not

$$\left|\Delta P_i^{(k)}\right| \le \varepsilon$$

$$\left|\Delta Q_i^{(k)}\right| \le \varepsilon$$

If these values are less than the specified accuracy, then go to step 9, otherwise go to step 5.

Step 5: Form the Jacobian matrix using current voltage estimates and power values.

Step 6: Solve the linear system (Eq. 2.50) via triangular factorization/Gaussian elimination.

Step 7: Update voltages:

$$\delta_i^{(k+1)} = \delta_i^{(k)} + \Delta\delta_i^{(k)} \tag{1.47}$$

$$\left|V_i^{(k+1)}\right| = \left|V_i^{(k)}\right| + \Delta\left|V_i^{(k)}\right| \tag{1.48}$$

Step 8: Repeat from Step 2 until convergence.

Step 9: Finalize with output results (voltages, angles, power flows).

1.8.1.3 Flowchart of Newton-Raphson method :

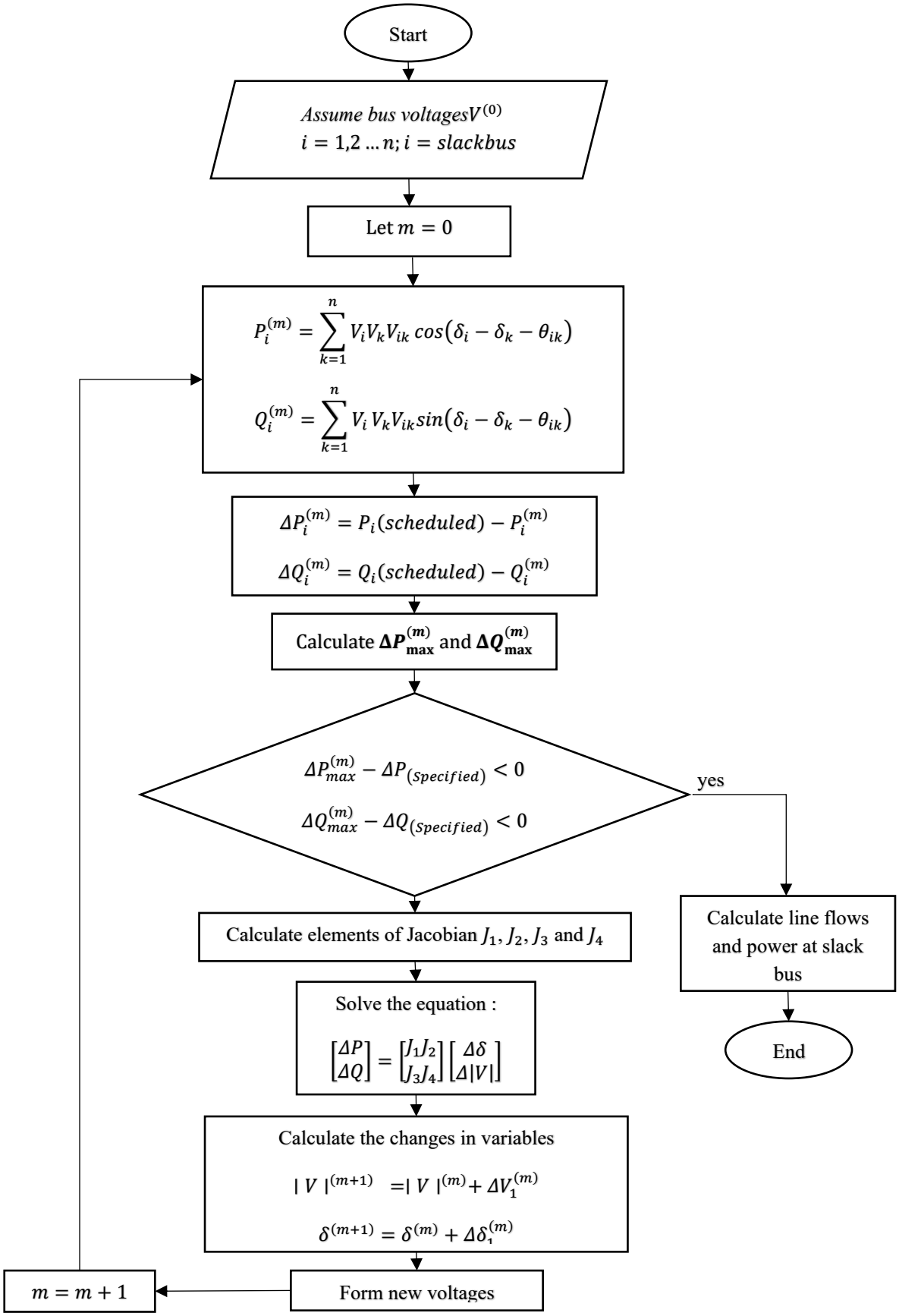

Figure 1. 6 : Flowchart of Newton-Raphson method [16].

1.8.2 Gauss sidel :

Gauss-Seidel (GS) method is an iterative technique used to solve the nonlinear power flow equations in electrical power systems. It updates bus voltages sequentially, using the most recent values as soon as they are available in each iteration.

Each bus voltage is updated sequentially using neighboring bus voltages to find the solution vector x that solves the nonlinear power flow equations. [17]

$$f(x) = 0 \tag{1.49}$$

can be reformulated like a fixed-point problem:

$$x = F(x) \tag{1.50}$$

whose solution, starting from the initial value x0 , is iteratively obtained through the sequence:

$$x_i^{k+1} = F_i\left(x_1^{k+1}, \dots, x_{i-1}^{k+1}, x_i^k, \dots, x_n^k\right) \quad i = 1,2, \dots, n \tag{1.51}$$

For the concrete case of load sharing, the solution of the nodal equation is such that:

$$V_i^{k+1} = \frac{1}{Y_{ii}}\left[\frac{P_i - jQ_i}{\left(V_i^k\right)^*} - \sum_{j=i}^{i-1} Y_{ij} \,.\, V_j^{k+1} + \sum_{j \neq i}^{n} Y_{ij} \,.\, V_j\right] \quad i = 1,2, \dots, n-1 \tag{1.52}$$

The iterative process is stopped when the condition:

$$max|V_i^{k+1} - V_i^k| \leq \varepsilon \tag{1.53}$$

The process can be enhanced by reducing the number of iterations using an acceleration factor α. [18]

$$V_{i,accl}^{k+1} = V_i^k + \alpha(V_i^{k+1} - V_i^k) \tag{1.54}$$

1.8.3 Fast decoupl :

The Fast Decoupled Load Flow (FDLF) method is based on the observation that, in most electrical systems, the submatrices J2 and J3 of the Jacobian matrix are approximately negligible compared to J1 and J4. This simplification allows equation (1.35) to be rewritten by decoupling the active and reactive power equations as follows: [14] [3] [6]

$$\begin{bmatrix}\Delta P\\ \Delta Q\end{bmatrix}=\begin{bmatrix}J_1 & 0\\ 0 & J_4\end{bmatrix}\begin{bmatrix}\Delta\delta\\ \Delta|V|\end{bmatrix} \tag{1.55}$$

$$\Delta P = J_1\Delta\delta = \left[\frac{\partial P}{\partial\delta}\right]\Delta\delta \tag{1.56}$$

$$\Delta Q = J_4\Delta|V| = \left[\frac{\partial Q}{\partial|V|}\right]\Delta|V| \tag{1.57}$$

From this equation, it is evident that the change in active power ΔP depends only on the change in phase angles $\Delta\delta$, and the change in reactive power ΔQ depends only on the change in voltage magnitudes $\Delta|V|$. This justifies the decoupling between [Pδ]and [QV].

In addition to setting the J_2 and J_3Jacobian submatrices to zero, the method relies on several simplifying assumptions: [6]

- $\cos(\delta_{ik}) \approx 1$
- $\sin(\delta_{ik}) \approx 0$
- $G_{ik}\sin(\delta_{ik}) \ll B_{ik}$
- $Q_i \ll B_{ii}V_i^2$, where B_{ii} is the total susceptance of all elements connected to node i.

It should be noted that these simplifications are not considered in heavily loaded electrical systems or those operating at lower voltage levels. Taking these approximations into account, the submatrices J_1 and J_4 become:

$$\begin{cases} J_1(i,i) = J_4(i,i) = -|V_i|^2 B_{ii} \\ J_1(i,k) = J_4(i,k) = -j|V_i||V_k|B_{ik} \end{cases} \tag{1.58}$$

Another simplification assumes that $|V_i| \approx |V_k| \approx 1$, *which leads to:*

$$\begin{cases} J_1(i,k) = -B_{ik}; & i = 2{:}n \quad k = 1{:}n \\ J_4(i,k) = -jB_{ik}; & i = m+1{:}n \quad k = m+1{:}n \end{cases} \tag{1.59}$$

This equation shows that the Jacobian matrix elements remain constant, which avoids recalculating them at each iteration. This significantly reduces computation time, hence the name “fast” method. Thus, equation (1.55) takes the following simplified form: [6]

$$\begin{cases} \left[\Delta P^{k'}\right] = B' \left[\Delta\delta^{k'}\right] \\ \left[\Delta Q^{k'}\right] = B'' \left[\Delta|V|^{k'}\right] \end{cases} \tag{1.60}$$

As follows:

$$\begin{cases} B'_{ik} = -B_{ik}; i = 2:n \quad k = 1:n \\ B''_{ik} = -B_{ik}; i = m+1:n \quad k = m+1:n \end{cases} \tag{1.61}$$

1.9 Conclusion :

In this chapter, we focused on presenting a clear understanding of the concept of "power flow" and the mathematical modeling of various components within an electrical network. The chapter also detailed the different types of buses and their specific characteristics, followed by a classification of power flow problems based on the solvability of equation systems including well-conditioned, ill-conditioned, bifurcation point, and unsolvable cases. We discussed the formulation of the power flow problem and the equations governing it, as well as the classification of the involved variables into disturbance, control, and state variables. Finally, the chapter explored various numerical methods for solving power flow problems, such as the Newton-Raphson method and the Fast Decoupled method, among others.

Chapter 2:

Optimal power flow

2.1 Introduction

Electric power grids are said to be the most intricate man-made systems because of their extensive geographic reach, numerous utility transactions, and the variety of layouts, sizes, and equipment employed by separate electric power firms. To properly analyse, monitor, and regulate many parts of such a complex system, engineers require specialised tools. Economic dispatch, unit commitment, state estimate, autonomous generation control, and optimum power flow (OPF) are a few of these techniques, I this chapter we focus on optimal power flow , and the probabilistic methods used to solve it under uncertainty. [19]

2.2 Optimization problems :

- An optimization problem may involve either a single objective (mono-objective) or multiple objectives , and is defined by a set of variables, one or more objective functions, and a set of constraints.
- The set of constraints are equalities or inequalities that restrict the search space. Optimization methods try to identify solutions that fulfill these constraints while optimizing the objective function.
- Total Active Transmission Losses, Voltage Deviation, and Voltage Stability Index, or even the objective function, specify the desired outcome, be it maximizing or minimizing. A unimodal function only has one minimum, the overall minimum, but a multimodal function contains several minima. [15]

2.3 Optimal power flow :

A power flow issue that minimizes or maximizes an objective function while meeting operational and physical restrictions is known as optimal power flow. is a mathematical optimization problem used in power system operations to find the most cost-effective, safe, and efficient method of generating dispatch while meeting operational and physical restrictions. OPF seeks to determine the best configurations for a given power system network that fulfil its equipment operating constraints, system security, and power flow equations while optimizing a certain objective function.[19]

2.4 The ORPD problem formulation :

The goal of the Optimal reactive power dispatch (ORPD) issue is to optimize system functioning by means of a particular objective function optimization under a set of equality and inequality constraints. Mathematically, the challenge may be stated as follows:

$$\begin{cases} \text{Min F(x, u)} \\ g(x,u) = 0\ (equality\ constraints) \\ h(x,u) \leq 0\ (inequality\ constraints) \end{cases} \quad (2.1)$$

2.4.1 Objective functions :

2.4.1.1 Total active transmission losses :

The following formulation can be used to minimize active power loss in the transmission lines [20]

$$P_{loss} = \sum_{k=1}^{NTL} g_k \left[V_i^2 + V_j^2 - 2V_iV_j\cos(\delta_i - \delta_j)\right] \quad (2.2)$$

P_{loss}: Total active power losses in the transmission system.

NTL: Number of transmission lines in the power system.

g_k: Conductance of the k^{th} transmission line .

V_i: Voltage magnitude at bus i.

V_j: Voltage magnitude at bus j.

δ_i: Voltage phase angle at bus i.

δ_j: Voltage phase angle at bus j.

2.4.1.2 Voltage deviation :

The objective is to minimize the voltage deviation of all load (PQ) buses from the nominal value of 1.0 p.u. This enhances the overall security of the power system and contributes to improved service quality. The objective function for voltage deviation minimization is mathematically expressed as: [21]

$$TVD = \sum_{i=1}^{NPQ} | V_{L,i} - 1 | \quad (2.3)$$

NPQ: Number of load buses .

2.4.1.3 Voltage stability index:

A power system is considered stable if it can keep all bus voltages within acceptable bounds. When the power system experiences significant disruptions, an increase in the electric demand, or changes in the network configuration, it enters a state of voltage instability, which results in a gradual and unanticipated voltage reduction. The improvement of the system voltage stability for each bus is a fundamental measure to ensure a safe and stable power system using voltage stability (L-index). Its value ranges from zero to one, where zero indicates no load and one indicates a voltage drop. In the event that the power system contains NPV generator buses (PV buses) and NPQ load buses (PQ buses), the L-index is assessed by [22]

$$L_j = \left| 1 - \sum_{i=1}^{N_{PV}} F_{ji} \frac{V_{Gi}}{V_{Lj}} \right| \quad j = 1,2,\dots,N_{PQ} \tag{2.4}$$

N_{PV}: Number of generator buses (PV buses).

where the complex voltages of the load bus j and the generation bus i are denoted by V_{Lj} and V_{Gi}, respectively.

$$F_{ji} = -[Y_{LL}]^{-1} \cdot [Y_{LG}] \tag{2.5}$$

The YBUS matrix was used to produce the sub-matrices Y_{LL} and Y_{LG} after nodal current injections were rearranged in relation to nodal voltages, which are defined as follows:

$$\begin{bmatrix} I_L \\ I_G \end{bmatrix} = \begin{bmatrix} Y_{LL} Y_{LG} \\ Y_{GL} Y_{GG} \end{bmatrix} \begin{bmatrix} V_L \\ V_G \end{bmatrix} \tag{2.6}$$

The following equation represents the system stability indicator, which is the maximum value (Lmax) of (Lj) among all load buses. It may be thought of as an objective function.

$$L_{max} = \max(L_j) \quad where \quad j = 1,2,\dots\dots,N_{PQ} \tag{2.7}$$

2.4.2 Constraints :

2.4.2.1 Equality Constraints :

The equality constraints of the ORPD show the physical rules controlling the electrical network. The non-linear power flow equations that call for the sum of the active and reactive powers injected at each busbar is zero [23] .

$$P_{Gi} - P_{Di} - V_i \sum_{j=i}^{NB} V_j \left[G_{ij}\cos(\theta_{ij}) + B_{ij}\sin(\theta_{ij})\right] = 0 \tag{2.8}$$

$$Q_{Gi} - Q_{Di} - V_i \sum_{j=i}^{NB} V_j \left[G_{ij}\sin(\theta_{ij}) + B_{ij}\cos(\theta_{ij})\right] = 0 \tag{2.9}$$

P_{Gi}: Active power generated .

Q_{Gi}: Reactive power generated .

P_{Di}: Active power demand .

Q_{Di}: Reactive power demand .

G_{ij}: Real part of the bus admittance matrix element .

B_{ij}: Real part of the bus admittance matrix element .

NB: Total number of buses in the system .

2.4.2.2 inequality constraints:

Physical and safety restrictions on the electrical network's component equipment are reflected in inequality limitations. The most prevalent restrictions include phase-shifting transformers, tapped transformers, busbar voltage limitations, and limits put in place to guarantee system safety.

Other inequality limitations must also be taken into account, such as compensator reactive power limits and power plant active and reactive power generation limits that must be kept at allowable levels.[23]

- **Generation Constraint:** Generator voltages, real power outputs, and reactive power outputs are restricted by their upper and lower bounds as follows[24]:

$$V_{G_i}^{min} \leq V_{G_i} \leq V_{G_i}^{max}, \quad i = 1, \dots, NG \tag{2.10}$$

$$P_{G_i}^{min} \leq P_{G_i} \leq P_{G_i}^{max}, \quad i = 1, \dots, NG \tag{2.11}$$

$$Q_{G_i}^{min} \leq Q_{G_i} \leq Q_{G_i}^{max}, \quad i = 1, \dots, NG \tag{2.12}$$

- **Transformer constraints**: Transformer tap settings ought to be restricted by their lower and upper limits as follows[25]:

$$T_i^{min} \leq T_i \leq T_i^{max}, \quad i = 1, \dots, NT \tag{2.13}$$

- **Shunt VAR compensator constraints** Shunt VAR compensations are restricted by their upper and lower bounds as follows [24]:

$$Q_{C_i}^{min} \leq Q_{C_i} \leq Q_{C_i}^{max}, \quad i = 1, \dots, NC \tag{2.14}$$

- **Security constraints**: include limitations on voltage magnitudes at PQ buses and the loading of transmission lines. The voltage at each PQ bus must remain within its specified minimum and maximum operating limits. Similarly, the power flow through each transmission line must not exceed its rated capacity. These constraints are detailed as follows. [21]

$$V_{L_i}^{min} \leq V_{L_i} \leq V_{L_i}^{max}, \quad i = 1, \dots, NL \tag{2.15}$$

$$S_{l_i} \leq S_{l_i}^{max}, \quad i = 1, \dots, Nl \tag{2.16}$$

2.5 Classification of methods:

Numerical methods for solving the optimal power flow "OPF" problem are classified into Figure 2.1 :

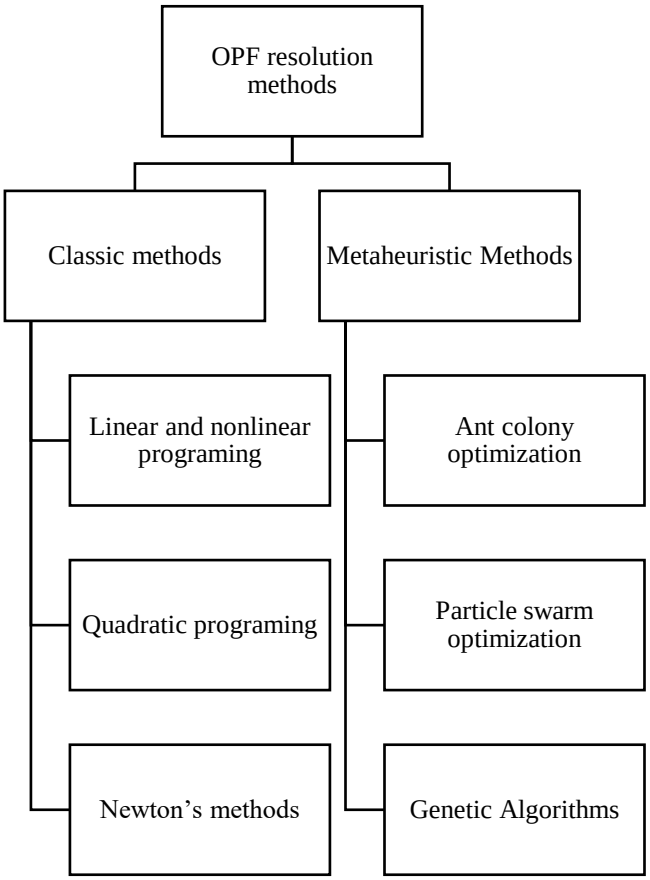

Figure 2. 1 :The OPF resulution methods.

2.5.1 classical method :

The classical methods are called deterministic or conventional optimization methods, are mathematical approaches that utilize gradient information to find optimal solutions, Common methods are Linear Programming and nonlinear [26], Quadratic Programming [27], Gradient Method [28], Newton's Method [27].

2.5.2 Metaheuristic Methods :

Global optimization methods, often referred to as metaheuristics, are inspired by natural processes. Some are based on evolutionary theory, like Genetic Algorithms (GA), while others draw from ethology, such as Swarm Intelligence methods like Particle Swarm Optimization (PSO) and Ant Colony Optimization (ACO). These algorithms use probabilistic and random exploration of the search space, which helps avoid getting trapped in local optima unlike deterministic methods that often struggle with complex or non-linear objective functions.

First introduced in the 1980s, metaheuristics originated in discrete problems but have since been adapted to continuous domains. They are typically used when traditional mathematical approaches fail to find satisfactory solutions. However, their performance is problem-dependent and influenced by algorithm parameters. Metaheuristics are widely applied in various fields, especially in electrical energy optimization [29] .

2.6 Optimal reactive power dispatch :

In power system operation, optimal reactive power dispatch (ORPD), one of the subproblems of the optimal power flow (OPF) computation, is crucial. The primary goal of ORPD is to determine the best control variable settings for minimizing the specified objective functions while meeting a number of system limitations for the whole dispatch time. Control variables include both continuous and discrete variables, such as generator voltages and reactive compensation capacity and transformer tap setings. also, system constraints are composed of two equality constraints and a set of inequality constraints. [30]

ORPD optimization problem formulations differ greatly depending on the particular selection of variables, objective(s) and constraints. Because of the specialized nature of ORPD[31], There are so many approaches have been proposed for optimal reactive power dispatch in a power system over the past decades. Conventional techniques like Mixed integer Programming, and evolutionary computation techniques. [32]

Traditionally, conventional methods have been effectively utilized to address ORPD (Optimal Reactive Power Dispatch) problems. These approaches are tailored to accommodate various objective functions and constraints. They rely on mathematical formulations that often need to be simplified to obtain optimal solutions. However, conventional methods exhibit several limitations, such as a restricted capability in solving large-scale, real-world optimization problems, inefficiency in constraint handling, slow convergence and potential stagnation, high computational time especially when dealing with a large number of variables and high costs associated with solving complex power system models . [31]

To address the limitations of traditional techniques, evolutionary methods and their hybrid variants have been developed and applied to ORPD problems in recent years. These methods offer several key advantages: a fast convergence rate, suitability for solving non-

linear optimization problems, the ability to find global optimum solutions, effectiveness in handling multi-objective optimization problems, capability to identify multiple optimal solutions in a single simulation run, and flexibility in managing constraints. [31]

For instance, the Particle Swarm Optimization PSO [33] algorithm and the Gravitational Search Algorithm GSA [34] have been widely used in ORPD studies due to their simplicity, robustness, and high efficiency in exploring the search space to find optimal solutions.

2.7 Uncertanty modeling :

To consider the uncertainties of the load demand and output powers of wind [35], There are different methods for modeling these uncertain parameters which are summarized in Figure (2.2) .

In this case we use the continuous probability density function (PDF) is used for modeling the uncertainties of the system where the PDF is divided into subsections to obtain a number of scenarios from the load demand, wind speed [36].

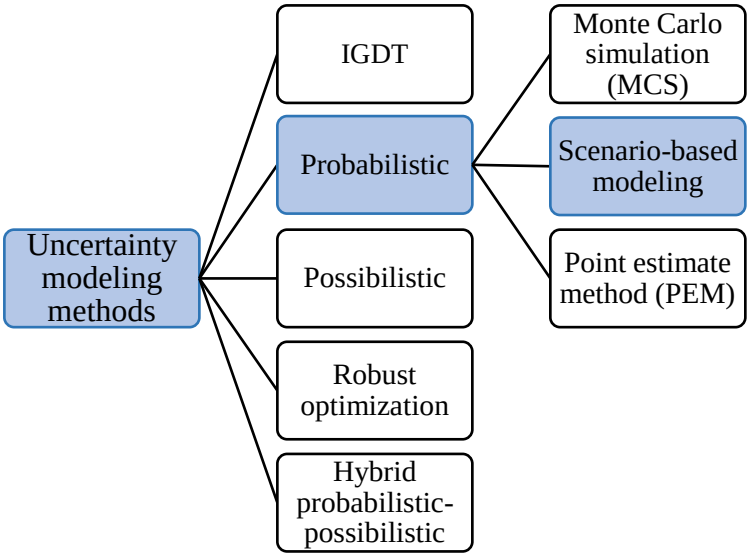

Figure 2. 2 : Uncertainty modeling methods.

2.7.1 Probabilistic approach:

The probabilistic method uses a multivariate function, $y = f(Z)$ where Z is a vector of the type $Z = [z_1, \ldots, z_m]$, where z_1 to z_m are random parameters with known PDFs while the PDF of Z is tried to be identified.

the function f describes the system model (set of load flow equations), Z is a vector of input uncertain parameters to the system (power injections by electric loads and wind energy), y is the output variable (total active losses for example). in this study we use the Probabilistic uncertainty via scenario based modelin. [37]

2.7.2 Uncertainty modelling via scenario-based approach:

2.7.2.1 Uncertainty for load demand :

Uncertainty of load demand is modeled using normal PDF which can be described as [35].

$$f_d(P_d) = \frac{1}{\sigma_d\sqrt{2\pi}} exp\left[-\frac{(P_d - \mu_d)2}{2\sigma_d^2}\right] \tag{2.17}$$

There is a considerable amount of uncertainty around the power system's predicted load. This structural uncertainty leads to the predicted load's (PDF) being divided into several intervals.

Figure (2.3) shows a normal predicted PDF of load that is divided into different periods. The analysis assumes known statistical parameters (μ_d, σ_d) obtained from forecasting tools and historical data. Each *i*th scenario's probability π_d and expected load value P_{D_i} serve as key data points for the study. [38]

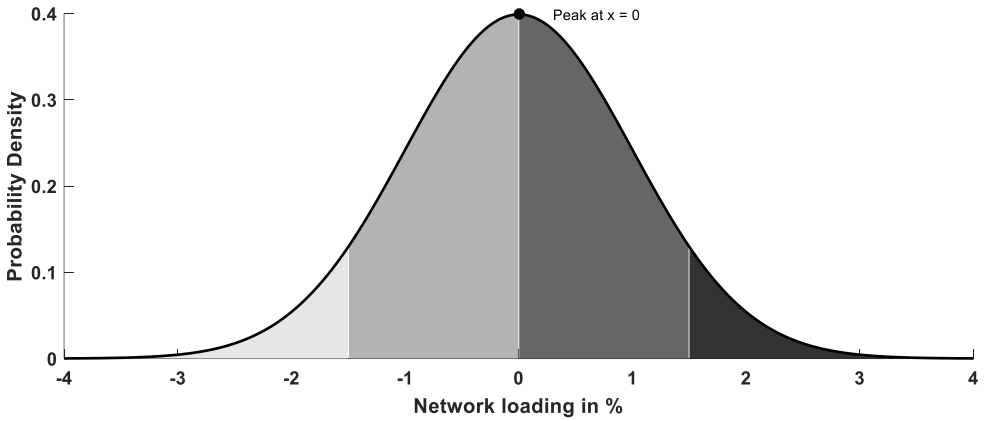

Figure 2. 3 : Typical discretisation of the PDF of the load.

calculated using Figure (2.2*)* as follows:

$$\pi_d = \int_{P_{D_d}^{\min}}^{P_{D_d}^{\max}} \frac{1}{\sqrt{2\pi\sigma_D^2}} \exp\left[-\frac{(P_D - \mu_D)^2}{2\sigma_D^2}\right] \mathrm{d}P_D \tag{2.18}$$

$$P_{D_i} = \frac{1}{\pi_d} \int_{P_{D,d}^{\min}}^{P_{D,d}^{\max}} \left(P_D \times \frac{1}{\sqrt{2\pi\sigma_D^2}} \exp\left[-\frac{(P_D - \mu_D)^2}{2\sigma_D^2} \right] \right) \mathrm{d}P_D \tag{2.19}$$

where N_{sc} is the total number of scenarios and π_d is the probability of a scenario . Similarly, expected power loss (EPL) are computed by:

$$\mathrm{EPL} = \sum_{sc=1}^{N_{sc}} \pi_d \times P_{\mathrm{loss,sc}} \tag{2.20}$$

2.7.2.2 Wind power generation uncertainty modelling :

In most cases, the Rayleigh or Weibul PDF is used to represent the uncertainty in wind speed . The Weibull distribution is a generalized version of the Rayleigh PDF. The wind speed's Rayleigh PDF can be expressed as follows[39]:

$$PDF(v) = \left(\frac{v}{c^2}\right) exp\left[-\left(\frac{v}{\sqrt{2}c}\right)^2 \right] \tag{2.21}$$

The wind speed variation range is divided into different intervals indicated, which are called scenarios

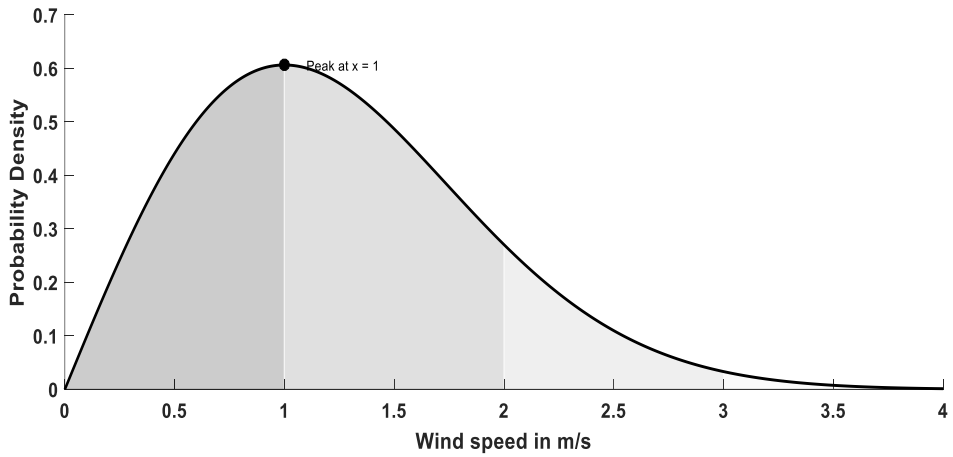

Figure 2. 4 : Rayleigh Distribution representation the uncertainty in wind speed

The occurrence probability of each scenario and its corresponding wind speed v_s are calculated as follows:

$$\pi_W = \int_{v_{i,w}}^{v_{f,w}} \left(\frac{v}{c^2}\right) exp\left[-\left(\frac{v}{\sqrt{2}c}\right)^2 \right] dv \tag{2.22}$$

$$v_W = \frac{1}{\pi_W} \times \int_{v_{i,w}}^{v_{f,w}} \left(v \times \left(\frac{v}{c^2}\right) exp\left[-\left(\frac{v}{\sqrt{2}c}\right)^2 \right] \right) dv \tag{2.23}$$

$v_{i,w}$ $v_{f,w}$ are the starting and ending points of the wind speed interval for the w-th scenario, v_W is the wind speed at the w-th wind scenario, and c is a scaling parameter obtained from historical wind speed data.

The characteristic curve of a wind turbine defines the relationship between the available wind speed and the corresponding generated wind power. A linearized characteristic curve is shown in Figure (2.5).

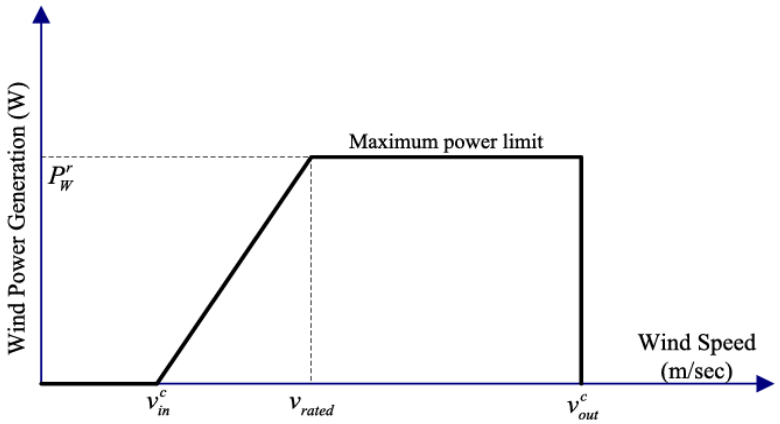

Figure 2. 5 : the power curve of a wind tubine.

The following formula may be used to determine the wind turbine's predicted output power based on this curve for a range of wind speed values:

$$P_W^{aul} = \begin{cases} 0 & v_w \le v_{in}^c or v_w \ge v_{out}^c \\ \dfrac{v_w - v_{in}^c}{v_{rated} - v_{in}^c} P_r^w & v_{in}^c \le v_w \le v_{rated} \\ P_r^w & v_{rated} \le v_w \le v_{out}^c \end{cases} \tag{2.24}$$

To model uncertainty in both wind power and load demand, a set of scenarios is generated for each. The total number of combined wind-load scenarios is obtained by multiplying the number of wind scenarios with the number of load scenarios. The probability of each combined scenario formed by the *w*th wind scenario and the *l*th load scenario can be calculated using the following expression [39] :

$$\pi_s = \pi_w \times \pi_d \tag{2.25}$$

2.8 Optimal reactive power dispatch with uncertainty :

Deterministic approaches to ORPD problems have been well developed and widely used in power systems. However, many uncertain factors exist during power system operations such as energy availability and power demands. An overestimation of the uncertainties can lead to conservative operations. In contrast, aggressive operations will probably lead to constraint violations. Different kinds of approaches have been proposed in the last few decades to deal with uncertainties in power systems. Prominent among these approaches are probabilistic methods which consider uncertain input variables as random inputs with known probability density functions (PDFs). Although probabilistic approaches require more sophisticated analysis, the benefits far outweigh the additional effort required to apply them.[40]

2.9 Conclusion :

This chapter presented the formulation of the Optimal Power Flow OPF problem, aiming to optimize the operation of power systems while satisfying technical and operational constraints. Different objective functions and constraint types were discussed, along with a classification of classical and metaheuristic solution methods. The Optimal Reactive Power Dispatch ORPD problem was also addressed.

Finally, the chapter emphasized the importance of uncertainty modeling using probabilistic scenario-based approaches to ensure a more reliable and realistic analysis of power system performance.

Chapter 3:

The hippopotamus optimization algorithm

3.1 Introduction :

In this chapter, we present the Hippopotamus Optimization Algorithm (HOA), a recent metaheuristic optimization technique inspired by the natural behavior of hippopotamuses. Metaheuristic algorithms are widely used for solving complex and nonlinear optimization problems where traditional methods often fail or become too expensive. These algorithms rely on intelligent strategies inspired by nature, physics, or social systems to explore the solution space effectively.

HO models the behaviors of hippopotamuses through three main phases: exploration, defense, and escape. Each phase represents a strategic way to search for optimal solutions, allowing the algorithm to balance global exploration with local exploitation. This balance helps HOA avoid local minima and find better solutions more efficiently. [41]

3.2 Hippopotamus :

The hippopotamus is one of the largest semi aquatic mammals in Africa, typically found in rivers and ponds. These animals are highly social and live in groups called pods or bloats, which usually consist of several females, their offspring, and a dominant male. Their behavior is a fascinating combination of curiosity, aggressiveness, and territorial instinct. Although they are herbivores, hippopotamuses are considered among the most dangerous animals due to their powerful jaws, unpredictable nature, and strong defense mechanisms. They are capable of producing loud warning vocalizations up to 115 decibels when threatened, and if intimidation fails, they can escape rapidly toward the nearest water source, moving at speeds up to 30 km/h. These instinctive behaviors exploring the environment, defending their territory, and escaping danger form the biological foundation upon which the Hippopotamus Optimization Algorithm (HOA) was developed, translating real life animal behavior into a computational strategy for solving complex optimization problems. [41]

3.3 Inspiration :

The HO is inspired by three key behavioral traits of hippopotamuses. First, hippopotamus herds typically consist of several females, calves, adult males, and one dominant male who leads the group. Young hippos, driven by curiosity, often wander away from the group, making them vulnerable to predators.

Second, hippos display a strong defensive instinct when threatened. They turn to face predators and use their powerful jaws and loud vocalizations to ward off attacks. Predators

like lions and hyenas are aware of this and usually avoid direct confrontations to prevent injury.

Lastly, when in danger, hippos often choose to flee rather than fight. They instinctively head for the nearest water source, such as a river or pond, since predators like lions and hyenas are generally reluctant to enter water. [41]

3.4 Mathematical modelling of HO :

The Hippopotamus Optimization (HO) algorithm is a population-based optimization technique, where the search agents are modeled as hippopotamuses. In this algorithm, each hippopotamus represents a candidate solution to the optimization problem, with its position update in the search space reflecting the values of the decision variables. Consequently, each hippopotamus is depicted as a vector, and the entire population is mathematically represented as a matrix. Much like traditional optimization algorithms, the initial stage of the HO algorithm involves generating randomized initial solutions. During this phase, the vector of decision variables is created using the following formula[41]:

$$\chi_i: x_{ij} = lb_j + \mathrm{r}.\left(ub_j - lb_j\right) \ , i = 1,2,\dots,N \qquad j = 1,2,\dots,m \tag{3.1}$$

χ_i: Represents the position of the *i-th* candidate solution (hippopotamus).

r: A random number in the range [0, 1].

lb_j and ub_j: Lower and upper bounds of the *j-th* decision variable.

N: Population size (number of hippopotamuses in the herd).

m: Number of decision variables in the optimization problem.

the population matrix is formed as follows:

$$\chi = \begin{bmatrix} \chi_1 \\ \vdots \\ \chi_i \\ \vdots \\ \chi_N \end{bmatrix}_{\mathcal{N}\times m} = \begin{bmatrix} x_{1,1} & \cdots & v_{1,j} & \cdots & x_{1,m} \\ \vdots & \ddots & \vdots & \ddots & \vdots \\ x_{i,1} & \cdots & x_{ij} & \cdots & x_{i,m} \\ \vdots & \ddots & \vdots & \ddots & \vdots \\ x_{N,1} & \cdots & x_{\mathcal{N},j} & \cdots & x_{\mathcal{N},m} \end{bmatrix}_{\mathcal{N}\times m} \tag{3.2}$$

3.4.1 Phase 1: The hippopotamuses position update in the river or pond (Exploration)

In hippopotamus herds, a dominant male leads a group consisting of adult females, calves, and other adult males. The leader is selected based on the objective function value, which is the lowest for minimization and highest for maximization problems.

Hippopotamuses tend to stay close together, with the dominant male protecting the herd. Mature males are eventually expelled and must compete or attract females to form their own group. [41]

This equation (3.3) represent the position of male hippopotamus members of the herd in the lake or pond :

$$\chi_i^{\mathcal{M}hippo}: x_{ij}^{\mathcal{M}hippo} = x_{ij} + y_1.\left(\mathcal{D}_{hippo} - I_1 x_{ij}\right) \tag{3.3}$$

$$for \qquad i = 1,2,\dots,\left[\frac{\mathcal{N}}{2}\right] \qquad and \qquad j = 1,2,\dots,m$$

$\chi_i^{\mathcal{M}hippo}$: Position of the *i-th* male hippopotamus (candidate solution).

$\mathcal{D}_{hippo}$: Position of the dominant hippopotamus (the best solution in the current iteration).

y_1 : is a random number between 0 and 1

$$h = \begin{cases} I_2 \times \vec{r}_1 + (\sim \varrho_1) \\ 2 \times \vec{r}_2 - 1 \\ \vec{r}_3 \\ I_1 \times \vec{r}_4 + (\sim \varrho_2) \\ r_5 \end{cases} \tag{3.4}$$

$\vec{r}_{1\dots4}$: Random vectors with values between 0 and 1.

r_5 : A random number between 0 and 1 .

$I_1\ and\ I_2$: is an integer between 1 and 2 .

ϱ_1 and ϱ_2 are integer random numbers that can be 1 or 0 .

$$T = \exp\left(-\frac{t}{T}\right) \tag{3.5}$$

$$\chi_i^{\mathcal{FB}^{hippo}} : x_{iji}^{\mathcal{FB}^{hippo}} = \begin{cases} x_{iji} + h_1.(\mathcal{D}_{hippo} - .I_2\mathcal{MG}_i) T > 0.6 \\ \Xi \end{cases} \quad (3.6)$$

$$\Xi = \begin{cases} x_{ij} + h_2.(\mathcal{MG}_i - \mathcal{D}hippee) r_6 > 0.5 \\ lb_j + r_7.(ub_j - lb_j) \quad \text{else} \end{cases} \quad (3.7)$$

$$for \qquad i = 1,2,\dots,\left[\frac{\mathcal{N}}{2}\right] \qquad and \qquad j = 1,2,\dots,m$$

h_1 and h_2 : are numbers or vectors randomly selected from the five scenarios in the h equation.

Equations (3.6) and (3.7) delineate the position of the female hippopotamus or the immature hippopotamus within the herd. Most of the time the immature hippopotamus is close to its mother; however, sometimes due to their curious nature, the immature separated from the herd or away from their mothers.

- When T > 0.6, the immature hippopotamus is found farther from the mother, as in Equation (3.5).
- When $r_6 > 0.5$, there has been distancing from the mother yet still within or near the herd, as in Equation (3.7).
- When $r_6 \leq 0.5$, the immature hippopotamus has distanced away from the herd, also described in Equation (3.7).

This behavior of female hippopotamuses and their immature offspring was modeled according to equations (3.6) and (3.7).

$$\chi_i = \begin{cases} \chi_i^{\mathcal{M}\text{hippo}} \mathcal{F}_i^{\mathcal{M}\text{hippo}} & < \mathcal{F}_i \\ \chi_i & else \end{cases} \quad (3.8)$$

$$\chi_i = \begin{cases} \chi_i^{\mathcal{FB}^{hippo}} \mathcal{F}_i^{\mathcal{FB}^{hippo}} & < \mathcal{F}_i \\ \chi_i & else \end{cases} \quad (3.9)$$

Equations (3.8), (3.9) describe male and female or immature hippopotamus position update within the herd. $\mathcal{F}_i$ is objective function value.

Employing h vectors, I_1 and I_2 scenarios strengthen the worldwide search and boost exploration in the suggested algorithm. It results in superior global search and amplifies the exploration process in the suggested algorithm.

3.4.2 Phase 2: Hippopotamus defence against predators (Exploration) :

Hippopotamus herding behaviour mainly ensures safety and security, as a large group can deter predators. Immature or sick individuals Hippopotamus that stray from the herd are more vulnerable to attacks by Nile crocodiles, lions, and spotted hyenas due to their limited defense capability.

The main defensive strategy used by hippopotamuses is to quickly pivot in the direction of the predator and make loud noises to deter the predator from getting near to them as we see in Figure (3.1). During this phase, Hippopotamuses may display a behavior where they approach a predator in order to intimidate it and prompt its withdrawal. [41]

The predator's position in the search space is expressed in this equation:

$$\mathcal{P}redator: \mathcal{P}redator_j = lb_j + \vec{r}_8.\left(ub_j - lb_j\right), j = 1,2,\dots,m. \tag{3.10}$$

$\vec{r}_8$: represents a random vector ranging from 0 to 1.

$$\vec{\mathcal{D}} = \left|\mathcal{P}redator_j - x_{ij}\right| \tag{3.11}$$

Where $\mathcal{D}$ is the distance of the *i-th* hippopotamus to the predator (uniform random number between 2 and 3)

During this period, the hippopotamus exhibits defensive behavior driven by $\mathcal{F}_{\mathcal{P}redator_j}$ to counter an attack. Based on Equation (3.12):

$$\chi_i^{\mathcal{H}_{hippo}\mathcal{R}} \cdot x_{ij}^{\mathcal{H}_{hippo}\mathcal{R}} = \begin{cases} \overrightarrow{RL} \oplus \mathcal{P}redator_j + \left(\frac{f}{(c - d \times \cos(2\pi g))}\right).\left(\frac{1}{\vec{D}}\right) \mathcal{F}_{\mathcal{P}redator_j} < \mathcal{F}_i \\ \overrightarrow{RL} \oplus \mathcal{P}redator_j + \left(\frac{f}{(c - d \times \cos(2\pi g))}\right).\left(\frac{1}{2 \times \vec{D} + \vec{r}_9}\right) \mathcal{F}_{\mathcal{P}redator_j} \geq \mathcal{F}_i \end{cases} \tag{3.12}$$

$$for \qquad i = \left[\frac{\mathcal{N}}{2}\right] + 1, \left[\frac{\mathcal{N}}{2}\right] + 2, \dots, \mathcal{N} \qquad and \quad j = 1,2,\dots,m$$

f: A uniform random number between 2 and 4.

c: A uniform random number between 1 and 1.5.

g: A uniform random number between −1 and 1.

$\vec{r}_9$.: A random vector of size 1 × m.

$\chi_i^{\mathcal{H}_{hippo\mathcal{R}}}$: is the position of the hippopotamus when facing the predator.

$\overrightarrow{RL}$ is a random vector with a Lévy distribution, used to simulate sudden changes in the predator's position during an attack.

- If $\mathcal{F}_{\mathcal{P}redator_j} < \mathcal{F}_i$: The predator is very close, and the hippopotamus will promptly turn and charge at it to force retreat.
- If $\mathcal{F}_{\mathcal{P}redator_j} > \mathcal{F}_i$: : The predator is far, so the hippopotamus will turn toward it but only move within a limited range to signal its presence in the territory.

hippopotamuses emit loud vocalizations and turn swiftly toward predators as we can see in Figure (3.1), sometimes even approaching them to force retreat.

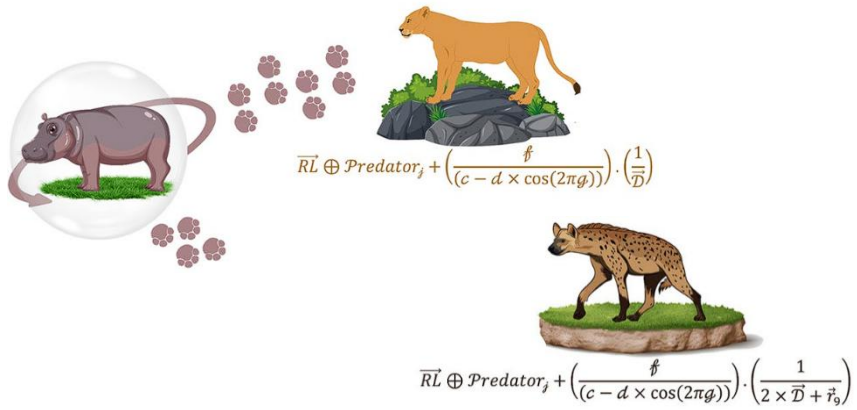

Figure 3. 1 : Hippopotamus Defensive Reaction Against a Predator [41].

The mathematical model for the random movement of Lévy movement is calculated in this equation , w and v are the random numbers:

$$\mathcal{L}evy(\vartheta) = 0.05 \times \frac{w \times \sigma_w}{|v|^{\frac{1}{\vartheta}}} \tag{3.13}$$

in [0,1], respectively ϑ is a constant (ϑ = 1.5),

σ_w can be obtained by Eq. (14). As follows :

$$\sigma_w = \left[\frac{\Gamma(1+\vartheta)\sin\left(\frac{\pi\vartheta}{2}\right)}{\Gamma\left(\frac{(1+\vartheta)}{2}\right)\vartheta 2^{\frac{(\vartheta-1)}{2}}}\right]^{\frac{1}{\vartheta}} \tag{3.14}$$

Γ is an abbreviation for Gamma function

$$\chi_i = \begin{cases} \chi_i^{\mathcal{H}_{hippo}\mathcal{R}} \mathcal{F}_i^{\mathcal{H}_{hippo}\mathcal{R}} < \mathcal{F}_i \\ \chi_i \mathcal{F}_i^{\mathcal{H}_{hippo}\mathcal{R}} \geq \mathcal{F}_i \end{cases} \quad (3.15)$$

According to Equation (3.15):

- If $\mathcal{F}_i^{\mathcal{H}_{hippo}\mathcal{R}} \geq \mathcal{F}_i \rightarrow$ The hippopotamus has been hunted, and another hippopotamus will replace it in the herd.
- Otherwise ($\mathcal{F}_i^{\mathcal{H}_{hippo}\mathcal{R}} < \mathcal{F}_i$) $\rightarrow$ The hunter escapes, and this hippopotamus returns to the herd.

Great improvements were noted in the global search process during the second phase. The two phases supplement each other in a way that drastically reduces the risk of one getting stuck in local minima.

3.4.3 Phase 3: Hippopotamus Escaping from the Predator (Exploitation) :

When a hippopotamus encounters multiple predators or fails to defend itself, it retreats to the nearest water source, as predators like lions and hyenas avoid entering water. This helps it find a nearby safe spot as we can see in figure (3.2). In Phase Three of the HO algorithm, this behavior is simulated by generating a random position near the current one to enhance local exploitation. When the newly created position improves the cost function value, it indicates that the hippopotamus has found a safer position near its current location and has changed its position accordingly. [41]

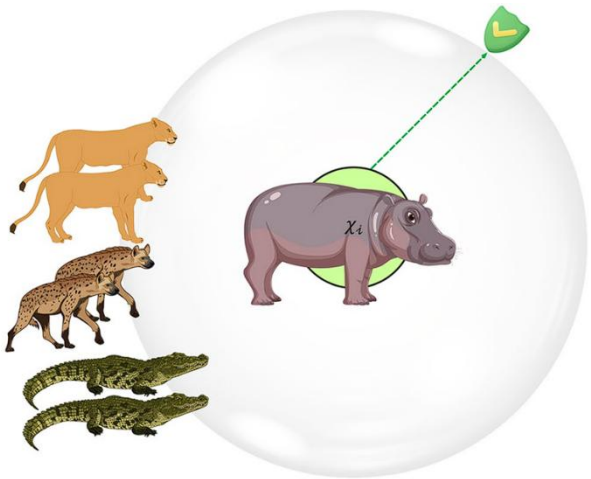

Figure 3. 2 : Hippopotamus Escaping Behavior from a Predator [41]

This behavior of the hippopotamuses is modelled according to the next equations :

$$lb_j^{local} = \frac{lb_j}{t} \qquad ub_j^{local} = \frac{ub_j}{t} \qquad t = 1,2,\dots,T \tag{3.16}$$

$$\chi_i^{\mathcal{H}_{ippo}\mathcal{E}} : x_{ij}^{\mathcal{H}_{ippo}\mathcal{E}} = x_{ij} + r_{10} \cdot \left(lb_j^{local} + s_1 \cdot \left(ub_j^{local} - lb_j^{local} \right) \right) \tag{3.17}$$

$$i = 1,2,\dots,\mathcal{N} \qquad j = 1,2,\dots,m$$

t denotes the current iteration and T represents the max iteration

$\chi_i^{\mathcal{H}_{ippo}\mathcal{E}}$ represents the position of the hippopotamus when searching for the nearest safe place.

s_1 is a random vector or number chosen from one of three predefined scenarios as we see in the next equation

$$s = \begin{cases} 2 \times \vec{r}_{11} - 1 \\ r_{12} \\ r_{13} \end{cases} \tag{3.18}$$

The considered scenarios s lead to a more suitable local search or in other words, result in the proposed algorithm having a higher exploitation quality.

$\vec{r}_{11}$ is a random vector with values between 0 and 1.

r_{10} (from Eq. 17) and r_{13} are random numbers also generated within the range [0, 1].

r_{12} is a random number following a normal distribution.

$$\chi_i = \begin{cases} \chi_i^{\mathcal{H}_{hippo}\mathcal{E}} \mathcal{F}_i^{\mathcal{H}_{hippo}\mathcal{E}} < \mathcal{F}_i \\ \chi_i \mathcal{F}_i^{\mathcal{H}_{hippo}\mathcal{E}} \geq \mathcal{F}_i \end{cases} \tag{3.19}$$

According to Equation (3.19):

- If $\mathcal{F}_i^{\mathcal{H}_{hippo}\mathcal{E}} \geq \mathcal{F}_i$:→ The hippopotamus has been hunted by the predators, and another hippopotamus will replace it in the herd.
- Otherwise ($\mathcal{F}_i^{\mathcal{H}_{hippo}\mathcal{E}} < \mathcal{F}_i$):→ The hippopotamus retreats to the nearest water source , and founded a safer position

In the HO algorithm for population updates, we avoided separating hippopotamuses into immature, female, and male groups. While this categorization would better reflect their natural behavior, it would negatively impact the optimization algorithm's effectiveness.

When each iteration of the HO algorithm concludes, the entire population undergoes updates through Phases 1 to 3. The population updating process following Equation (3.19), persists until reaching the final iteration. Throughout the algorithm's execution, the most promising solution is continuously monitored and recorded. Once the algorithm completes its full run, the optimal candidate, known as the dominant hippopotamus solution, emerges as the final answer to the problem. The HO step-by-step implementation is illustrated in Figure (3.3) flowchart pseudocode.

3.5 Flowchart of hippopotamus optimization method:

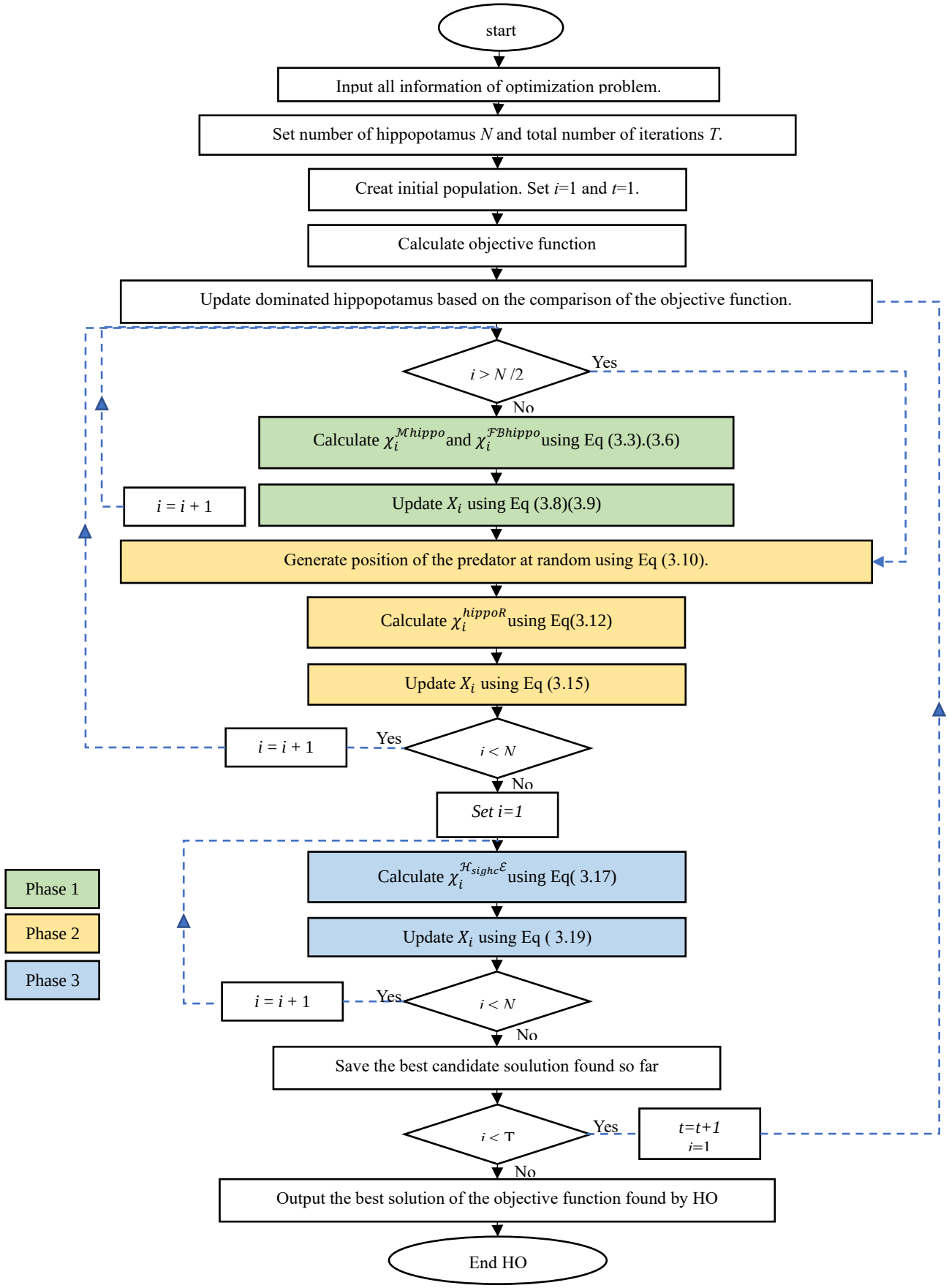

Figure 3. 3 : Flowchart of HO[41]

3.6 conclusion :

This chapter introduced the Hippopotamus Optimization Algorithm HO, a bio inspired metaheuristic algorithm modeled after the natural behaviors of hippopotamuses. HO operates in three main phases exploration, defense, and escape, each designed to simulate specific real life behaviors for efficient search and optimization. The algorithm balances global exploration and local exploitation through mathematical models based on herd dynamics, predator avoidance, and retreat strategies. The chapter detailed the implementation process, equations, and flowchart, demonstrating HO potential as a powerful tool for solving complex optimization problems.

Chapter 4:

Simulation results and analysis

4.1 Introduction :

This chapter presents the simulation results using the Optimization HO method, a metaheuristic technique applied to solve the Optimal Reactive Power Dispatch ORPD problem. The analysis begins with a deterministic approach under fixed load and generation conditions, using the modified IEEE 30-bus and 57-bus test systems. The outcomes are compared with those of another metaheuristic methods to evaluate the effectiveness of the proposed meta-heuristic optimization technique. Next, a probabilistic approach is introduced to account for uncertainties in load demand and wind power generation using a scenario-based framework. In this analysis, four distinct scenarios are employed to model load variations, while wind power fluctuations are represented through four additional scenarios, each assigned a specific probability of occurrence. This approach facilitates a more realistic evaluation of system behavior, operational stability, and the effectiveness of the proposed optimization method under uncertain conditions.

4.2 Simulation results and discussions :

To assess the effectiveness of the Hippopotamus Optimization Algorithm HO in solving the Optimal Reactive Power Dispatch ORPD problem, two standard IEEE test systems are considered: IEEE 30-bus and IEEE 57-bus. The optimization objective is to minimize the total active power losses (Ploss), Total Voltage Deviation TVD and enhancing the voltage stability index VSI. Table 4.1 presents the characteristics of the test systems and control paramater setting of HO.

Table 4. 1 : the characteristics of the test systems and control paramater setting of HO.

Characteristics	IEEE 30 bus	IEEE57 bus
Number of control variables	19	25
Number of Generators	6	7
Number of Taps	4	15
Number of Q-shunt	9	3
total active power demand (MW)	283.40	1250.80
total reactive power demand (MVAr)	126.20	336.40
Ploss (MW)	5.81	28.462
control paramater of HO		
Search Agents	80	150
Max iterations	150	300

4.3 IEEE 30 bus system :

To initiate the application of the proposed optimization approach to the ORPD problem, the IEEE 30-bus system is first considered. This network consists of 30 buses, a total of 19 control variables are included in the optimization process , 6 generators voltage magnitudes in buses 1; 2; 5; 8; 11 and 13 ranging from 0.95 to 1.10 per unit ,4 tap setting transformers T_{6-9}, T_{6-10}, T_{4-12} and T_{28-27}, ranging from 0.95 to 1.10 per unit , and 9 shunt reactive power injections in buses 10; 12; 15; 17; 20; 21; 23; 24 and 29, between 0 and 5 Mvar.

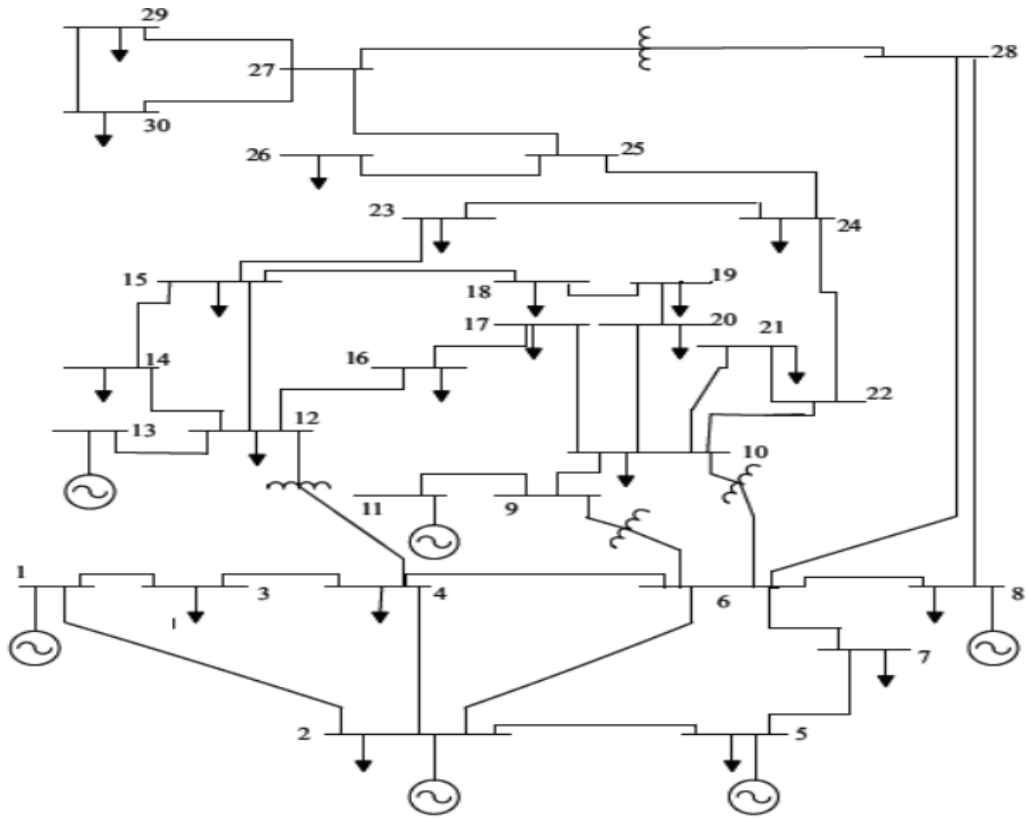

Figure 4. 1 :diagram of IEEE 30 bus power system [42]

4.3.1 Active Power Losses Minimization for IEEE 30 bus System :

In this case, the active total power losses was selected as the objective function to be minimized. The optimal control variables obtained from running the HO computing code are presented in Table 4.2. The results obtained after the simulation phase using the HO method are compared to other methods, such as PSO , CLPSO and ABC .The HO algorithm demonstrated superior performance , achieving a minimum Ploss of (4.5250 MW). This result surpasses those obtained by comparative algorithms, CLPSO (4.5615 MW), PSO (4.6282 MW), and ABC (4.7157 MW) As shown in same table 4.2 .

Specifically, HO achieved a 0.80% reduction compared to CLPSO, a 2.23% reduction compared to PSO, and a 4.04% reduction compared to ABC .

Table 4. 2 :Comparison of Ploss Minimization Results Using HO and Other Methods for IEEE 30-Bus.

Control variables	HO	ABC [15]	PSO [33]	CLPSO [33]
Generator voltage				
V_1 (p.u)	1.1000	1.0578	1.1000	1.1000
V_2 (p.u)	1.0946	1.0565	1.1000	1.1000
V_5 (p.u)	1.0751	1.0236	1.0867	1.0795
V_8 (p.u)	1.0770	1.0176	1.1000	1.1000
V_{11} (p.u)	1.0998	1.0426	1.1000	1.1000
V_{13} (p.u)	1.1000	1.0686	1.1000	1.1000
Transformer tap ratio				
T_{6-9}	1.0567	1.0380	0.9587	0.9154
T_{6-10}	0.9029	1.0289	1.0543	0.9000
T_{4-12}	0.9937	1.0755	1.0024	0.9000
T_{28-27}	0.9758	1.0396	0.9755	0.9397
Capacitor banks				
Q_{c-10} (MVAr)	2.5360	2.7614	4.2803	4.9265
Q_{c-12} (MVAr)	4.9878	2.0468	5.0000	5.0000
Q_{c-15} (MVAr)	3.9655	0.9966	3.0265	5.0000
Q_{c-17} (MVAr)	4.9571	2.7687	4.0365	5.0000
Q_{c-20} (MVAr)	3.5763	4.5165	2.6697	5.0000
Q_{c-21} (MVAr)	5.0000	3.3702	3.8894	5.0000
Q_{c-23}(MVAr)	3.5134	3.5046	0.0000	5.0000
Q_{c-24}(MVAr)	4.7590	2.4227	3.5879	5.0000
Q_{c-29}(MVAr)	2.8799	3.8632	2.8415	5.0000
P_{loss} (MW)	**4.5250**	**4.7157**	**4.6282**	**4.5615**
TVD (p.u)	2.4546	0.4789	1.0883	0.4773
L-index(p.u)	0.1272	0.1452	0.1423	0.1230

Furthermore, the convergence curve illustrated in the Figure 4.2 show a smooth evolution of the global best solution without any stagnation, demonstrating HO's capability to overcome premature convergence issues.

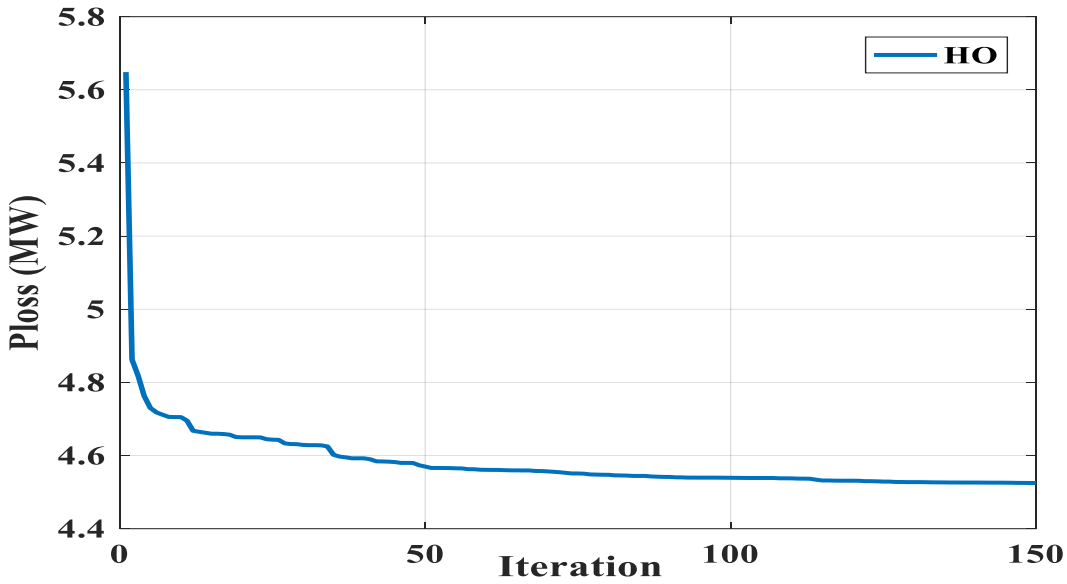

Figure 4. 2 :Convergence Curve of the HO Algorithm for Active Power Loss Minimization in the IEEE-30 Bus System.

• Figure 4.3 illustrates the voltage profile corresponding to objective functions in the IEEE 30-bus system upon reaching the optimal solution. It is observed that the voltage magnitudes at all buses remain within their permissible limits, also the figure 4.4 presents the actual reactive power generation values in MVAR for the generating units compared to their allowable limits, in which all generating reactive powers are within their limits.

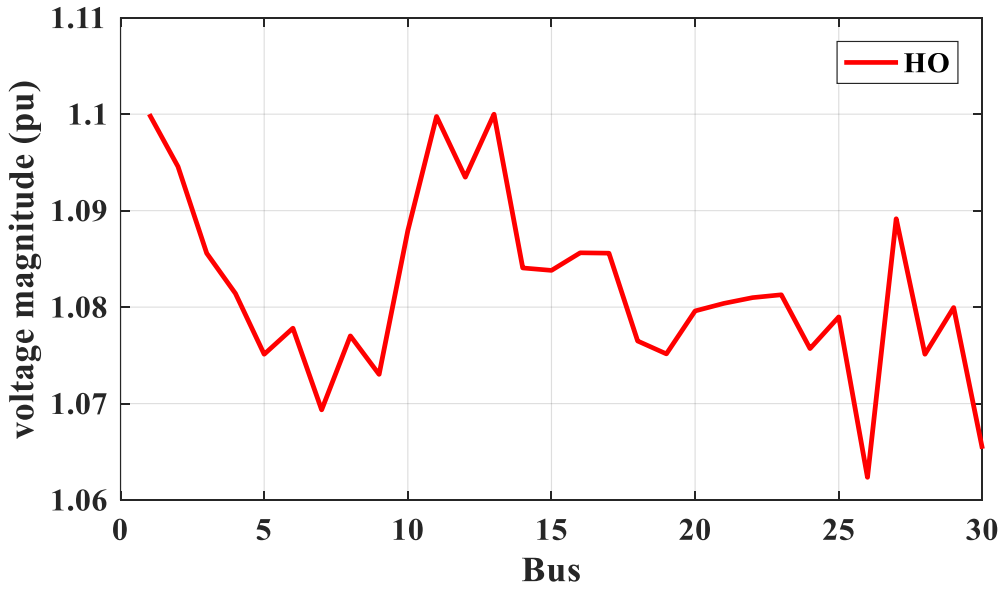

Figure 4. 3 : Bus voltage profile for IEEE 30 bus power system.

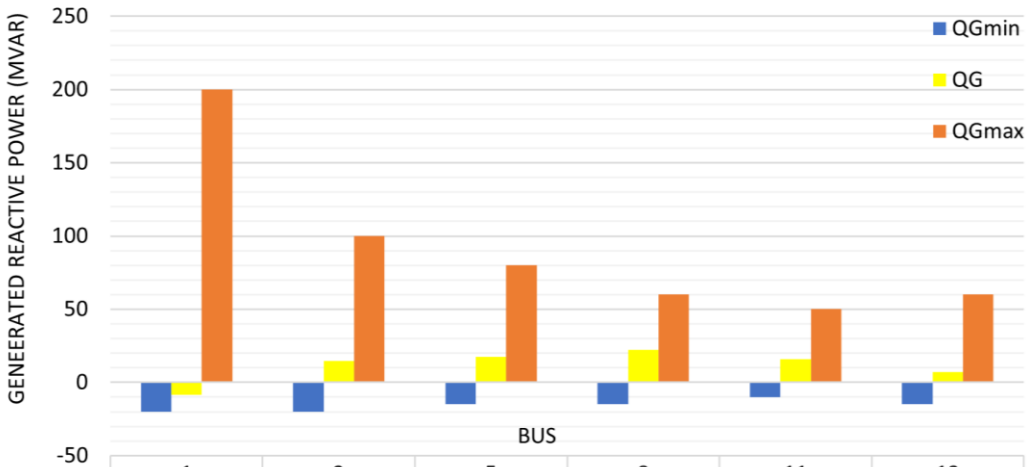

	1	2	5	8	11	13
QGmin	-20	-20	-15	-15	-10	-15
QG	-8.2507	14.6973	17.4908	22.2928	16.0072	6.9392
QGmax	200	100	80	60	50	60

Figure 4. 4 : Generated reactive power related to their minimum and maximum permissible limits in the IEEE 30-bus test system.

4.3.2 TVD Minimization for IEEE 30 bus System :

In this subsection, Total Voltage Deviation TVD was selected as the objective function to be minimized in the IEEE 30-bus system. Table 4.3 Table 4.3 clearly presents the optimal results achieved by the proposed HO algorithm in comparison with other optimization methods, namely PSO, CLPSO, and APO. The HO algorithm successfully achieved a minimum TVD value of (0.1631 p.u), outperforming both PSO (0.2577 p.u), and CLPSO (0.2450 p.u), while APO reached an even lower TVD of (0.1001 p.u). These results correspond to reductions of 36.7% relative to PSO and 33.4% relative to CLPSO for HO, and an additional 38.6% reduction when comparing APO to HO. The convergence behavior, illustrated in Figure 4.5, demonstrates a fast decrease in TVD values during the initial iterations, followed by a smooth and stable convergence towards the optimal solution

Table 4. 3 : Comparison of TVD Minimization Results Using HO and Other Methods for IEEE 30-Bus.

Control variables	HO	PSO [33]	CLPSO [33]	APO [43]
Generator voltage				
V_1 (p.u)	1.0003	1.0508	1.1000	1.0211
V_2 (p.u)	1.0006	1.0359	1.1000	1.0110
V_5 (p.u)	1.0001	1.0281	1.0724	1.0110
V_8 (p.u)	1.0233	1.0438	1.0764	0.9981
V_{11} (p.u)	1.0001	1.0306	1.0452	1.0411
V_{13} (p.u)	1.0000	1.0539	1.1000	0.9814
Transformer tap ratio				
T_{6-9}	0.9697	1.0020	1.0177	1.0512
T_{6-10}	0.9169	0.9003	0.9738	0.8912
T_{4-12}	0.9470	0.9825	1.0244	0.9327
T_{28-27}	0.9573	0.9958	0.9896	0.9612
Capacitor banks				
Q_{c-10} (MVAr)	1.8563	5.0000	0.7220	4.9652
Q_{c-12} (MVAr)	2.1695	4.4032	1.6812	0.0000
Q_{c-15} (MVAr)	3.8260	3.5695	2.6462	4.9681
Q_{c-17} (MVAr)	0.7654	4.2684	3.4105	4.9967
Q_{c-20} (MVAr)	3.2653	4.3108	1.9773	4.8456
Q_{c-21} (MVAr)	2.7753	4.8788	0.4767	4.8745
Q_{c-23} (MVAr)	3.1850	3.0728	3.5896	4.9974
Q_{c-24} (MVAr)	4.7002	3.8790	2.9998	4.9964
Q_{c-29} (MVAr)	2.1633	5.0000	1.1098	4.9781
P_{loss} (MW)	6.3493	4.7075	4.6969	5.4890
TVD (p.u)	**0.1631**	**0.2577**	**0.2450**	**0.1001**
L-index(p.u)	0.1472	0.1273	0.1247	0.1482

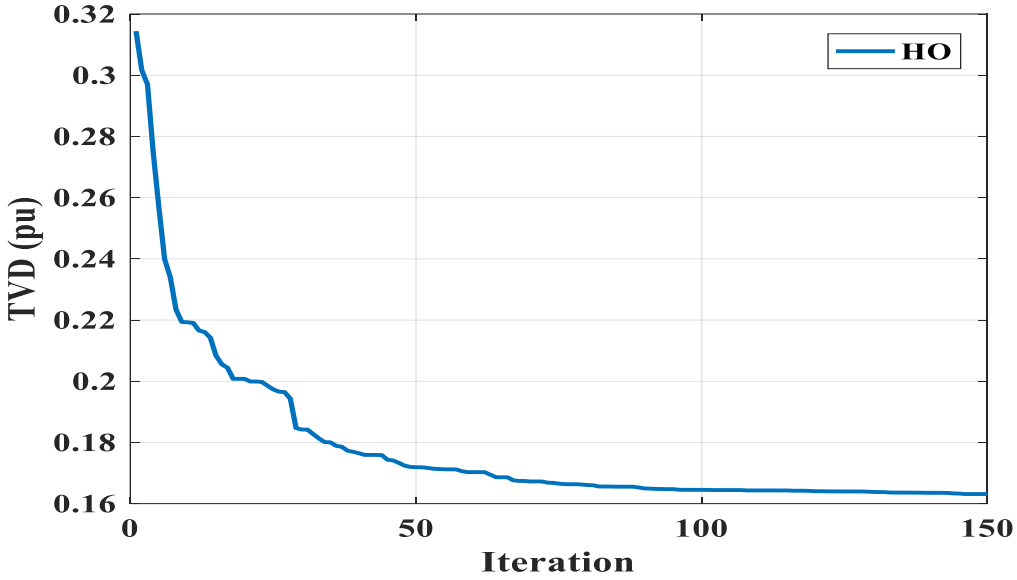

Figure 4. 5 : Convergence Curve of the HO Algorithm for TVD Minimization in the IEEE-30 Bus System.

4.3.3 VSI Improvement for IEEE 30 bus system :

In this case, the voltage stability index, represented by the L-index, was chosen as an objective function to be minimized using the HO algorithm. The simulation results are summarized in Table 4.4 and compared by other optimization methods, including ABC, SSA, and GSA. The HO algorithm achieved a minimum VSI value of (0.1098 p.u), outperforming ABC (0.1138 p.u), SSA (0.1139 p.u), and GSA (0.1160 p.u). As shown in the same table 4.4, This corresponds to relative improvements of 3.52%, 3.60%, and 5.34%, respectively, thereby affirming the superiority of the HO algorithm in enhancing system voltage stability. The convergence profile illustrated in Figure 4.6 exhibits a fast initial decline in VSI during the early iterations, stabilizing around the 50th iteration. The absence of oscillations or premature convergence in the subsequent iterations reflects the robustness of the HO algorithm in consistently locating and maintaining a high quality optimal solution.

Table 4. 4 : Comparison of improvement VSI Results Using HO and Other Methods for IEEE 30-Bus.

algorithms	HO	ABC [15]	SSA [15]	GSA [34]
P_{loss} (MW)	5.1696	5.4268	4.6581	6.6602
TVD (p.u)	3.8634	1.8551	2.0349	0.9000
L-indix (p.u)	**0.1098**	**0.1138**	**0.1139**	**0.1160**

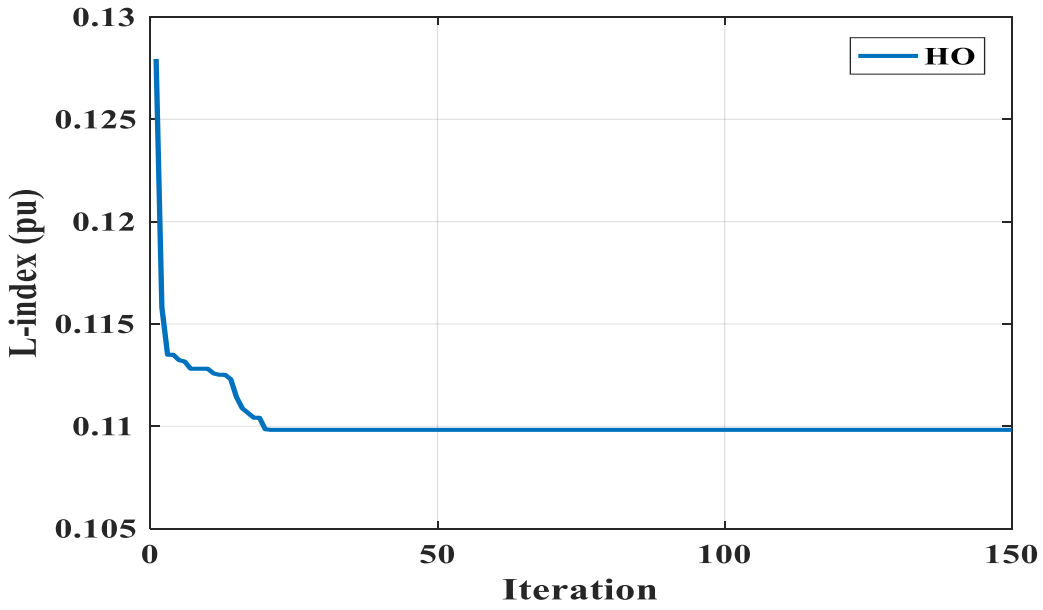

Figure 4. 6 : Convergence Curve of the HO Algorithm for VSI Minimization in the IEEE-30 Bus System.

4.4 IEEE 57 bus system :

The IEEE 57-bus system is considered as a more extensive and complex benchmark system for testing the proposed optimization approach in solving ORPD problem, which is illustrated in Fig 4.7. This network comprises 57 buses, and a total of 25 control variables are involved in the optimization process. These include 7 generator voltage magnitudes at buses 1, 2, 3, 6, 8, 9, and 12, bounded between 0.95 and 1.10 per unit, and 15 tap-setting transformers, T_{4-18}, T_{4-18}, T_{21-20}, T_{24-26}, T_{7-29}, T_{34-32}, T_{11-41}, T_{15-45}, T_{14-46}, T_{10-51}, T_{13-49}, T_{11-43}, T_{40-56}, T_{39-57}, T_{9-55}, with tap settings ranging from 0.90 to 1.10; and 3 shunt reactive power compensators located at buses 18, 25 and 53, with reactive power injection limits from 0 to 5 Mvar.

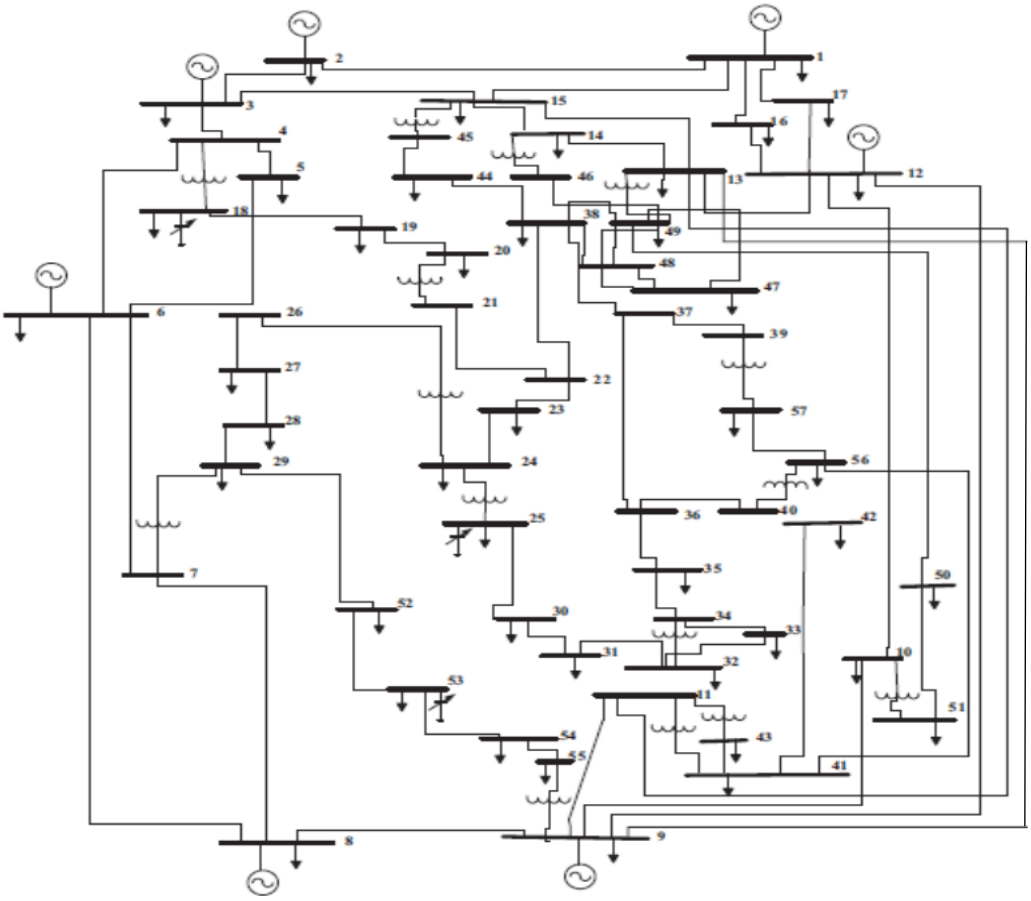

Figure 4. 7 : Diagram of IEEE 57 bus power system [42].

4.4.1 Active power losses Ploss minimization for IEEE 57 bus system :

The total active power losses Ploss are minimized in this case For the IEEE 57-bus power system. The optimal set of control variables determined through the execution of the HO code is detailed in Table 4.3. after the simulation process, the performance of the HO method was benchmarked against other optimization techniques such as ABC, SSA, and GSA. The HO algorithm demonstrated superior performance, achieving a minimum Ploss of (21.7057 MW). This result outperforms those obtained by ABC (23.3301 MW), SSA (23.4026 MW), and GSA (23.4619 MW), as shown in the same table 4.5. Specifically, HO achieved a 6.96% reduction compared to ABC, a 7.25% reduction compared to SSA, and a 7.49% reduction compared to GSA. Furthermore, the convergence curve illustrated in Figure 4.8 shows a fast decrease in early iterations for power losses, followed by a smooth and stable convergence. This behavior indicates a well-balanced exploration and exploitation process, confirming the robustness and efficiency of the HO algorithm in solving the ORPD problem, particularly in large-scale systems such as the IEEE 57-bus.

Table 4. 5 : Comparison of Ploss Minimization Results Using HO and Other Methods for IEEE 57-Bus.

Control variables	HO	ABC [15]	SSA [15]	GSA [34]
Generator voltage				
V_1 (p.u)	1.1000	1.1000	1.1000	1.0600
V_2 (p.u)	1.0994	1.0910	1.0906	1.0600
V_3 (p.u)	1.0887	1.0807	1.0825	1.0600
V_6 (p.u)	1.0830	1.0786	1.0736	1.0081
V_8 (p.u)	1.1000	1.0956	1.0996	1.0549
V_9 (p.u)	1.0851	1.0820	1.0710	1.0098
V_{12} (p.u)	1.0804	1.0901	1.0801	1.0158
Transformer tap ratio				
T_{4-18}	0.9068	0.7285	0.9732	1.1000
T_{4-18}	0.9066	0.3201	0.9832	1.0826
T_{21-20}	1.0004	0.8644	0.9710	0.9219
T_{24-26}	0.9881	0.6107	1.0450	1.0167
T_{7-29}	0.9001	0.2245	1.0041	0.9962
T_{34-32}	0.9494	0.3963	0.9638	1.1000
T_{11-41}	0.9000	0.1285	1.0118	1.0746
T_{15-45}	0.9002	0.2605	0.9646	0.9543
T_{14-46}	0.9001	0.1609	0.9726	0.9377
T_{10-51}	0.9122	0.1746	1.0282	1.0167
T_{13-49}	0.9000	0.0184	0.9621	1.0525
T_{11-43}	0.9009	0.1218	0.9464	1.1000
T_{40-56}	0.9787	0.5815	1.0042	0.9799
T_{39-57}	1.0241	0.4266	0.9595	1.0246
T_{9-55}	0.9000	0.3725	1.0451	1.0373
Capacitor banks				
Q_{c-18} (MVAr)	0.0632	1.0000	2.0440	0.0782
Q_{c-25} (MVAr)	4.0631	1.0000	1.9894	0.0058
Q_{c-53} (MVAr)	4.9820	1.0000	22.7681	0.0468
P_{loss} (MW)	**21.7057**	**23.3301**	**23.4026**	**23.4611**

TVD (p.u)	7.1595	2.7278	2.0268	-
L-index(p.u)	0.2281	0.3498	0.2762	-

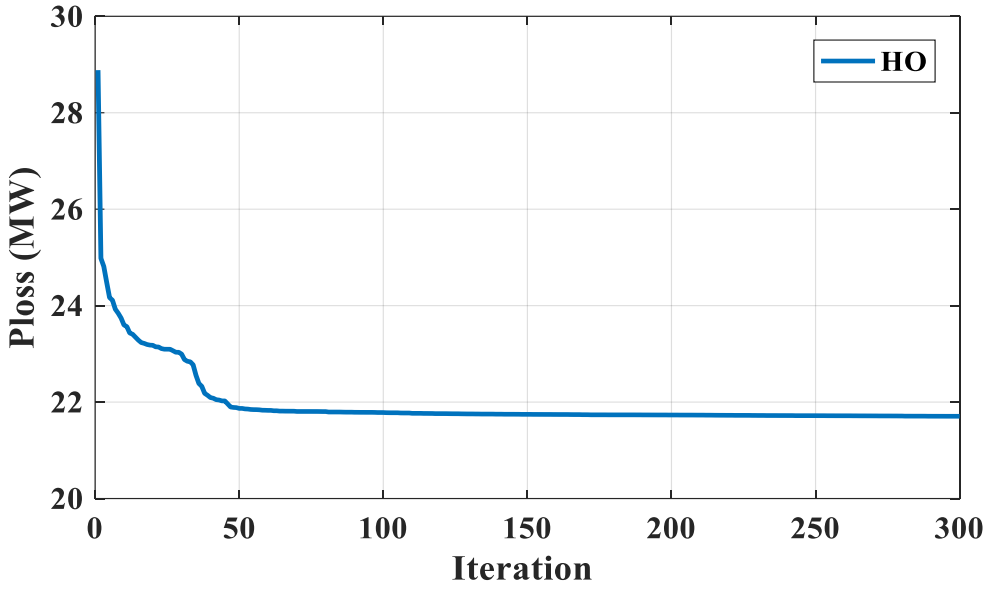

Figure 4.8 : Convergence Curve of the HO Algorithm for Active Power Loss Minimization in the IEEE-57 Bus System

• Figure 4.9 illustrates the voltage profile associated with the objective functions in the IEEE 57-bus system upon reaching the optimal solution. It shows that the voltage magnitudes at all buses remain within their permissible limits. and Figure 4.10 presents the actual reactive power generation values (in MVAr) of the generating units compared to their allowable limits. It is observed that all reactive power outputs remain within the specified operational boundaries.

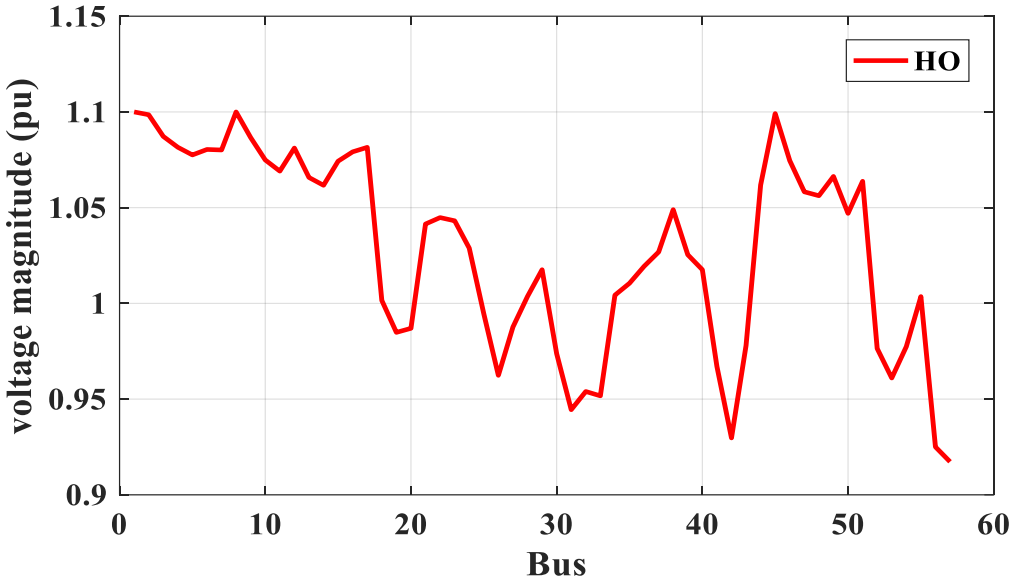

Figure 4.9 : Bus voltage profile for IEEE 57 bus power system.

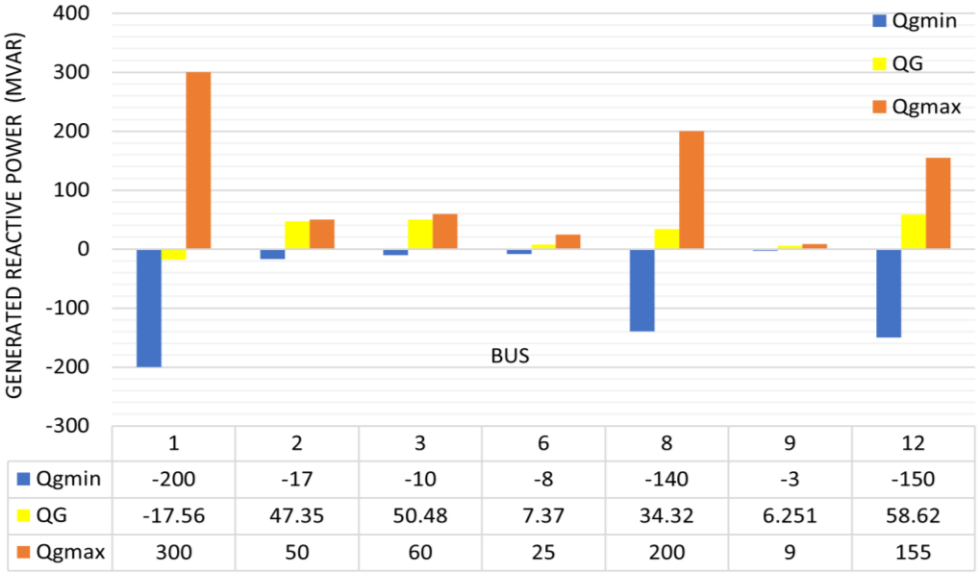

	1	2	3	6	8	9	12
Qgmin	-200	-17	-10	-8	-140	-3	-150
QG	-17.56	47.35	50.48	7.37	34.32	6.251	58.62
Qgmax	300	50	60	25	200	9	155

Figure 4. 10 :Generated reactive power related to their minimum and maximum permissible limits in the IEEE 57-bus test system

4.4.2 TVD Minimization for IEEE 57 bus System :

The Total Voltage Deviation TVD minimization was also carried out for the IEEE 57-bus power system to further assess the performance of the HO algorithm. The corresponding results are summarized in Table 4.6, which provides a comparison among HO, GSA, APOPSO, and ABC algorithms. The HO algorithm achieved a TVD value of (0.7874 p.u), outperforming GSA (1.1100 p.u) and APOPSO (0.9430 p.u), but was slightly outperformed by ABC, which obtained the lowest TVD of (0.7125 p.u). Specifically, HO achieved a 29.08% reduction in TVD compared to GSA and a 16.49% reduction compared

to APOPSO. However, ABC achieved a 9.51% lower TVD compared to HO. These results indicate that while HO demonstrates competitive performance and effective voltage control, The convergence curve depicted in Figure 4.11 further confirms the stability and efficiency of the HO algorithm. It shows a steep initial decline in TVD values during the early iterations, followed by a smooth and steady convergence towards the final solution. This behavior reflects a well balanced exploration and exploitation process.

Table 4. 6 : Comparison of TVD Minimization Results Using HO and Other Methods for IEEE 57-Bus.

algorithms	HO	GSA [34]	APOPSO [43]	ABC [15]
P_{loss} (MW)	28.3438	24.441	28.989	39.3993
TVD (p.u)	**0.7874**	**1.11**	**0.943**	**0.7125**
L-indix (p.u)	0.2984	-	0.1827	0.6825

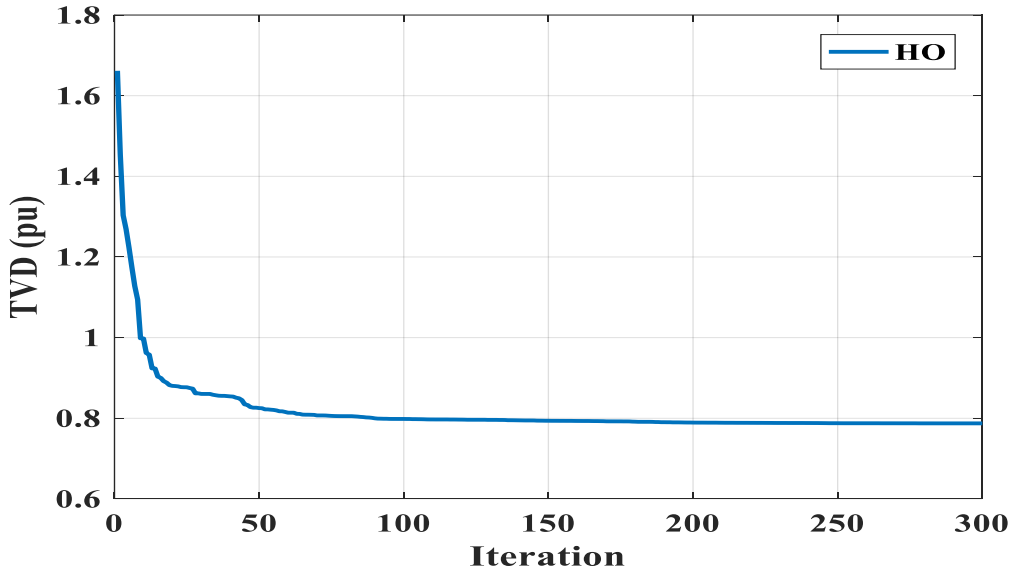

Figure 4.11 : Convergence Curve of the HO Algorithm for TVD Minimization in the IEEE-57 Bus System.

4.4.3 VSI Improvement for IEEE 57 bus system :

To evaluate the effectiveness of the proposed Hippopotamus Optimization Algorithm HO in enhancing voltage stability, a comprehensive simulation was conducted on the IEEE 57-bus system. The optimal control variables obtained from running the HO computing code are presented in Table 4.7. The HO algorithm achieved a minimum L-index value of (0.2088 p.u), outperforming the ABC and SSA algorithms, which recorded values of (0.2210 p.u) and (0.2360 p.u), respectively As shown in the same table .These results

represent improvements of approximately 5.52% compared to ABC and 11.52% compared to SSA. Such performance highlights the ability of the HO algorithm to maintain voltage stability more effectively. The convergence profile illustrated in Figure 4.12 further supports the effectiveness of the proposed Hippopotamus Optimization Algorithm HO. It demonstrates a rapid reduction in the L-index value during the early iterations, with the algorithm stabilizing around its optimal solution after approximately 100 iterations. This behavior indicates that the HO algorithm not only achieves a lower VSI value but does so efficiently, requiring fewer iterations to converge.

Table 4.7 : Comparison of improvement VSI Results Using HO and Other Methods for IEEE 57-Bus.

algorithms	HO	ABC [15]	SSA [15]
P_{loss} (MW)	57.1125	25.8623	25.1841
TVD (p.u)	8.1007	7.2551	3.4526
L-indix (p.u)	**0.2088**	**0.2210**	**0.2360**

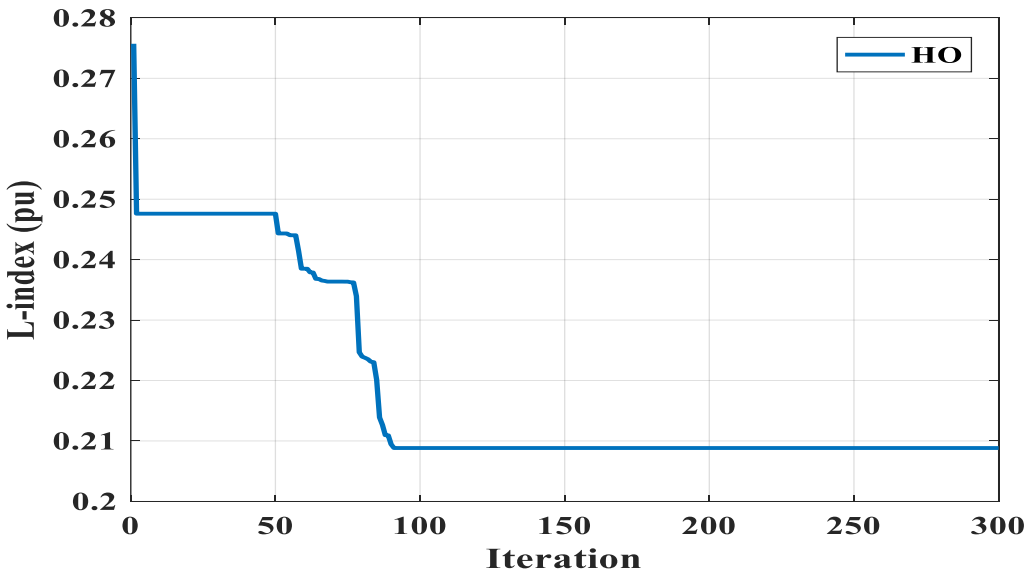

Figure 4.12 : Convergence Curve of the HO Algorithm for VSI Minimization in the IEEE-57 Bus System.

4.5 Results of optimal reactive power dispatch under load demand Uncertainties:

4.5.1 Scenario modeling of load variation :

In our study, we used scenario-based probabilities to model the variation in load demand as it occurs in real-life conditions. To represent this variation, we employed a Probability Density Function (PDF), which was divided into four distinct periods, as illustrated in Figure 4.13. with each period indicated by a different color. The analysis is based on known statistical parameters: the mean load demand μ_d, which corresponds to the peak value considered to be 70, and the standard deviation σ_d, set to 10.

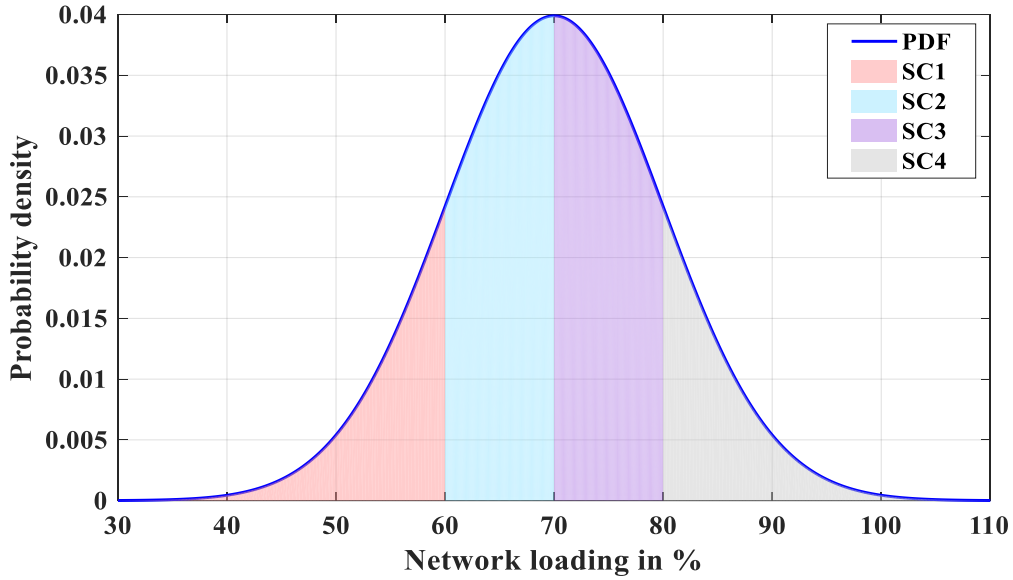

Figure 4.13 : : PDF of load uncertainty with μ_d= 70 , and standard deviation σ_d = 10

The calculated means and probabilities for all scenarios of loading are provided in Table 4.8 below:

Table 4.8 : load scenarios and their probabilities.

Loading scenario	loading P_{D_i}	Scenario probability π_d
Scenario 1	54.754%	0.15862
Scenario 2	65.401%	0.34134
Scenario 3	74.599%	0.34134
Scenario 4	85.246%	0.15862

As we can see ,each scenario corresponds to a specific loading percentage and has an associated probability. Scenarios 2 and 3, which are closest to the mean load demand (70%), have the highest probabilities (34.134%), while Scenarios 1 and 4, have lower

probabilities (15.862%). This distribution reflects the normal behavior of load variation around the average.

4.5.2 Simulation results and discussion of load variation :

Based on the application of the Hippopotamus Optimization Algorithm (HO) under load deman uncertnety , the simulation results for each load variation scenario are summarized in Table 4.9. These scenarios were examined with the objective of minimizing active power losses Ploss across the power system.

Table 4.9 : Effect of Load Demand Variation on Active Power Loss (Ploss) in Four Scenarios.

Control variables	Scenario1	Scenario 2	Scenario 3	Scenario 4
Generator voltage				
V_1 (p.u)	1.0939	1.0978	1.1000	1.1000
V_2 (p.u)	1.1000	1.1000	1.1000	1.0983
V_5 (p.u)	1.0957	1.0922	1.0895	1.0838
V_8 (p.u)	1.0940	1.0915	1.0893	1.0843
V_{11} (p.u)	1.0545	1.0243	1.0730	1.0998
V_{13} (p.u)	1.0845	1.0696	1.1000	1.0718
Transformer tap ratio				
T_{6-9}	0.9993	1.0973	1.0212	0.9748
T_{6-10}	0.9773	0.9281	0.9467	1.0904
T_{4-12}	1.0068	1.0209	1.0003	1.0249
T_{28-27}	1.0116	1.0186	0.9880	1.0025
Capacitor banks				
Q_{c-10} (MVAr)	3.2856	4.8187	2.9505	1.7180
Q_{c-12} (MVAr)	4.9500	1.3368	1.6474	4.8271
Q_{c-15} (MVAr)	4.7323	4.9262	3.5094	4.2541
Q_{c-17} (MVAr)	3.5299	4.9448	4.9444	4.9284
Q_{c-20} (MVAr)	1.2801	4.5521	4.9790	2.9836
Q_{c-21} (MVAr)	1.6130	4.9710	3.4200	4.5350
Q_{c-23} (MVAr)	4.6078	1.0372	0.6873	3.0734
Q_{c-24} (MVAr)	3.6240	4.9740	5	3.0985

Q_{c-29} (MVAr)	3.2974	1.5413	1.3400	1.8637
P_{loss} MW	**0.7929**	**0.9630**	**1.4700**	**2.4951**
TVD (pu)	2.5845	2.0471	2.6101	2.0751
L-index(pu)	0.0680	0.0850	0.0930	0.1117
EPL	**1.3520**			

Scenario 1, with the lowest load demand (54.754%), results in an active power loss representing the amount of real power dissipated in the system of (0.7929 MW). Scenario 2, reflects 65.401% of load demand, shows a slightly higher loss of (0.9630 MW), which is an increase of approximately 21.5% compared to Scenario 1.

Scenario 3, at 74.599% of nominal load, yields a loss of (1.4700 MW), marking an increase of around 52.7% from Scenario 2.

Scenario 4, at the highest load case with 85.246% of nominal load, shows the largest power loss at (2.4951 MW), which is approximately 69.7% higher than Scenario 3.

the Expected Power Loss (EPL), calculated using the probability of each scenario, is (1.2280 MW), representing the average loss expected under normal load variations.

- The simulation results confirm that all voltage magnitudes (Vm) across the buses remain within the acceptable limits, typically between 1.02 p.u and 1.10 p.u, as shown in Figure 4.14. No voltage violations were observed under any of the considered scenarios (Sc1 to Sc4), ensuring voltage security across the system.

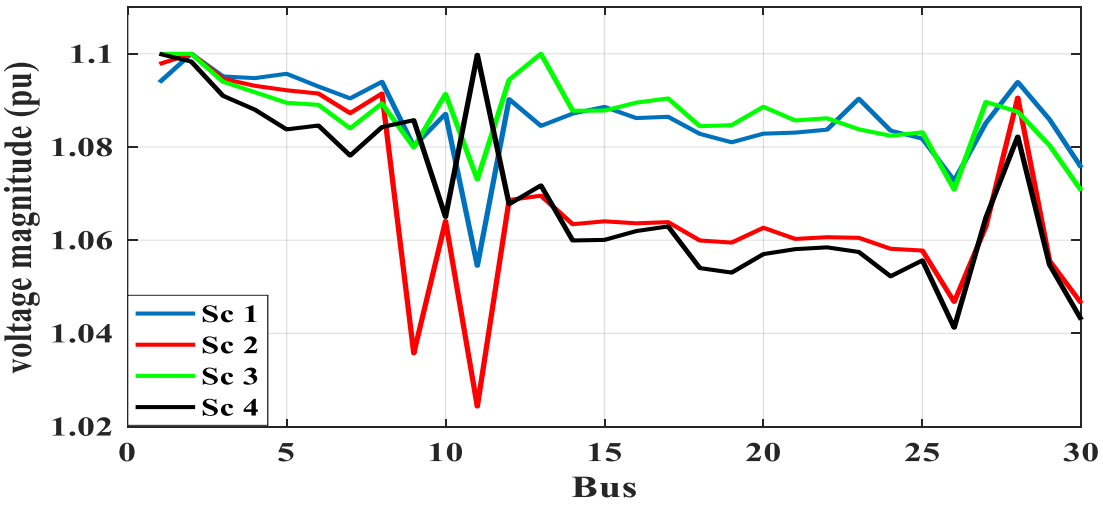

Figure 4.14 : Bus voltage magnitude profiles for IEEE 30-bus system under four different load demand scenarios.

- The generated reactive power Qg values for the main generator buses also stayed within their specified lower and upper bounds,as shown in Figure 4.15. Even under

uncertainty conditions, none of the scenarios led to Qg values exceeding their corresponding limits, which indicates that the proposed optimization approach successfully maintained all control variables within feasible operating ranges.

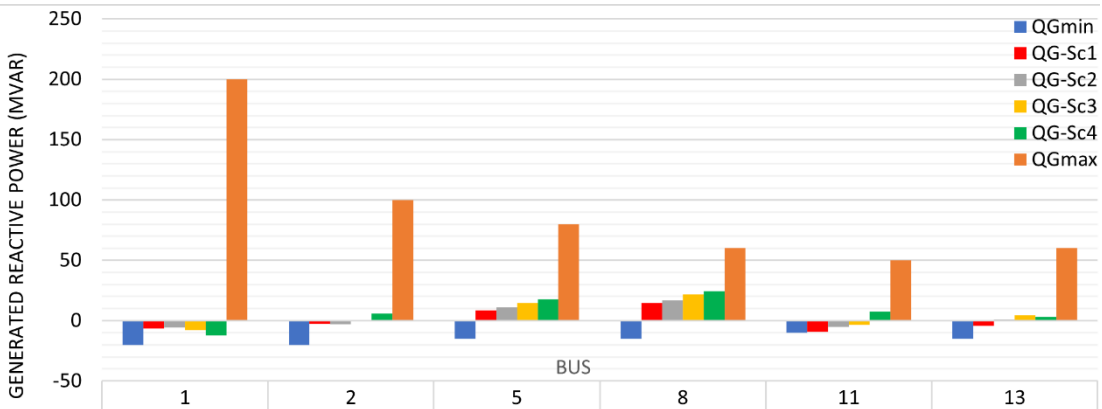

	1	2	5	8	11	13
QGmin	-20	-20	-15	-15	-10	-15
QG-Sc1	-6.4031	-2.6668	8.5887	14.8848	-9.2026	-4.2165
QG-Sc2	-5.7522	-3.1198	11.1594	16.8202	-5.2299	0.9453
QG-Sc3	-7.9814	-0.3562	14.5435	21.6496	-3.1933	4.6057
QG-Sc4	-12.0816	5.7159	17.5688	24.2935	7.773	3.3369
QGmax	200	100	80	60	50	60

Figure 4.15 : Generated reactive power related to their minimum and maximum limits in the IEEE 30-bus test system under four load demand scenarios.

4.6 Results of optimal reactive power dispatch under wind power uncertainties:

4.6.1 Scenario modeling of wind power variation :

To study the impact of uncertainty in wind power generation, a wind farm consisting of 15 wind turbines was integrated at bus 24. This analysis focuses on the probabilistic variation in wind speed, modeled using the Rayleigh probability density function (PDF), which is commonly used to represent wind speed distributions. Based on this model, four representative scenarios were selected, each one is characterized by wind speed interval and illustrated with a unique color in Figure 4.16**.** These scenarios allow for a realistic assessment of the wind farm's behavior under varying wind conditions. The inclusion of probabilistic modeling ensures a more robust and accurate evaluation of the system's performance under uncertainties.

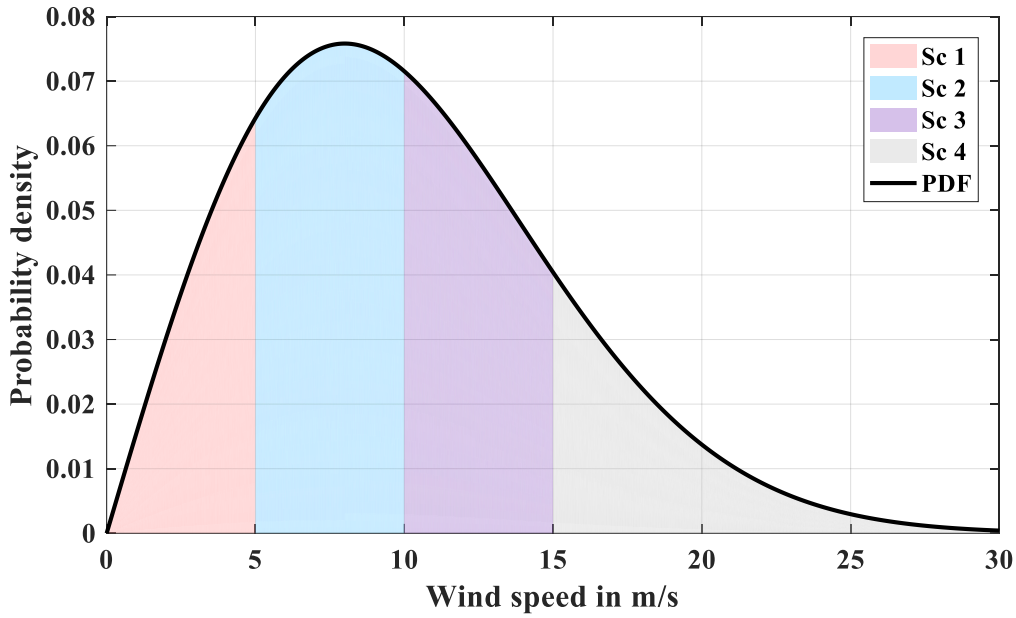

Figure 4.16 : Wind Speed Distribution Profiles for Scenarios Sc1 to Sc4 with c= 8 m/s.

The table 4.10 displays each scenario together with its associated probability of wind speed and the wind power generated in each scenario :

Table 4.10 : wind speed and their probabilities.

Loading scenario	Wind v_w (m/s)	Scenario probability π_w	WPG in single wind turbine(MW)	WPG entire wind farm (MW)
Scenario 1	3.268	0.17742	0.080	1.2
Scenario 2	7.539	0.36474	1.362	20.43
Scenario 3	12.267	0.28541	2.700	40.5
Scenario 4	18.466	0.17154	2.700	40.5

As we can see, Scenario 1, presents a low-wind speed, of (3.268 m/s) and wind farm generate only (1.2 MW). Scenario 2 is the most probable, has the highest probability (36.474%) and a wind speed of (7.539 m/s), produces (20.43 MW). Scenarios 3 and 4, with wind speeds of (12.267 m/s) and (18.466 m/s) respectively, both reach the maximum total wind power generation of (40.5 MW). This data clearly demonstrates how variations in wind speed significantly influence overall power output.

4.6.2 Simulation results and discussion of wind power variation :

Based on the implementation of the Hippopotamus Optimization Algorithm HO under wind power uncertainty, the simulation results corresponding to each operating scenario are presented in Table 4.11. These scenarios were investigated with the primary objective of minimizing active power losses Ploss

Table 4. 11 : Effect of wind speed Variation on Active Power Loss in Four Scenarios.

Control variables	Scenario1	Scenario 2	Scenario 3	Scenario 4
Generator voltage				
V_1 (p.u)	1.1000	1.1000	1.1000	1.1000
V_2 (p.u)	1.0948	1.0958	1.0971	1.0976
V_5 (p.u)	1.0758	1.0773	1.0789	1.0802
V_8 (p.u)	1.0779	1.0809	1.0848	1.0856
V_{11} (p.u)	1.1000	1.0765	1.0955	1.0929
V_{13} (p.u)	1.1000	1.1000	1.0896	1.0899
V_{24} (p.u)	1.0730	1.0973	1.1000	1.1000
Transformer tap ratio				
T_{6-9}	0.9440	1.0376	1.0857	1.0107
T_{6-10}	1.0570	0.9013	0.9018	0.9782
T_{4-12}	1.0091	0.9928	0.9926	0.9955
T_{28-27}	0.9907	0.9809	0.9974	0.9959
Capacitor banks				
Q_{c-10} (MVAr)	0.4645	5.0000	4.8534	3.7931
Q_{c-12} (MVAr)	4.9584	4.4765	4.8004	4.9968
Q_{c-15} (MVAr)	4.4279	3.3201	3.3692	3.3783
Q_{c-17} (MVAr)	2.9112	4.1607	5.0000	4.3582
Q_{c-20} (MVAr)	4.2597	3.9213	1.9859	3.7214
Q_{c-21} (MVAr)	4.9965	3.9301	4.3462	4.9986
Q_{c-23} (MVAr)	4.8416	4.7516	4.2637	4.1783
Q_{c-29} (MVAr)	4.6367	3.5303	4.1164	3.6521
P_{loss} MW	**4.4769**	**3.3717**	**2.9516**	**2.9444**
TVD (p.u)	2.3951	2.5942	2.5066	2.5254

L-index(p.u)	0.0848	0.0830	0.0844	0.0844
EPL	**3.3703**			

Scenario 1, with a probability of 17.742%, results in the highest active power loss at (4.4769 MW), reflecting poor operational efficiency. Scenario 2, the most likely at 36.474%, reduces Ploss to (3.3717 MW), indicating an approximate 24.7% reduction in power losses related to Scenario 1. Scenarios 3 and 4 achieve the lowest losses at around (2.95 MW), indicating optimal control performance where system losses are minimized and voltage profiles better maintained.

In general, the active power losses decreases with more injected active wind power. The Expected Power Loss (EPL) across all scenarios is (3.2338 MW), representing the average system loss under uncertain wind conditions

- Under wind power uncertainty, Figure 4.17 shows the voltage profile for each optimal state (related to each scenario) indicate that all bus voltage magnitudes Vm remain within permissible operational limits, which ensures voltage stability and power system security.

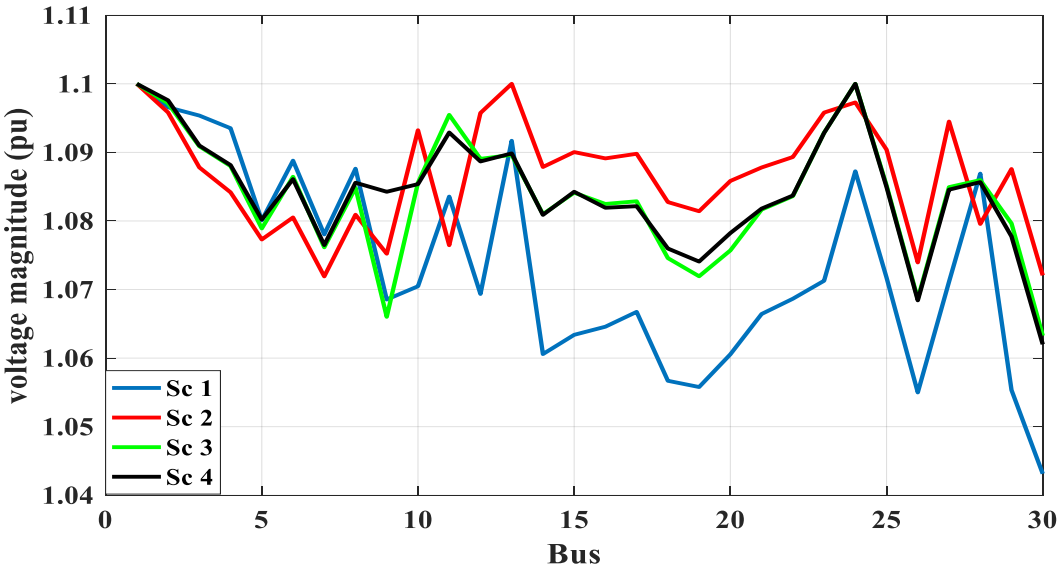

Figure 4.17 : Bus voltage magnitude profiles for IEEE 30-bus system under four different wind speed scenarios.

- The generated reactive power Qg at generator buses remains within specified limits across all scenarios as we can see in Figure 4.18. This confirms that the optimization method maintains feasibility and ensures system stability, even under wind uncertainty.

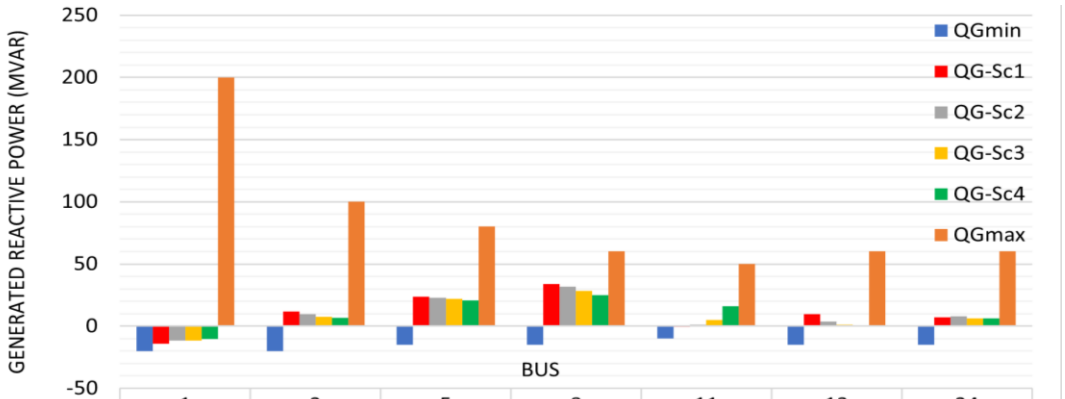

	1	2	5	8	11	13	24
QGmin	-20	-20	-15	-15	-10	-15	-15
QG-Sc1	-14.0698	11.7531	23.5648	33.8339	-0.001	9.6025	7.3143
QG-Sc2	-11.6892	9.7757	22.7466	31.5696	0.9994	3.573	7.7946
QG-Sc3	-11.3656	7.6433	22.0102	28.4217	4.8918	1.1492	6.4645
QG-Sc4	-10.428	6.5428	20.6712	25.0373	15.8716	0.6852	6.4645
QGmax	200	100	80	60	50	60	60

Figure 4.18 : Generated reactive power related to their minimum and maximum limits in the IEEE 30-bus test system under four wind speed scenarios.

4.7 Simulation results and discussion of wind/load uncertainties :

In this case of study, both wind power and load demand uncertainties were jointly considered to generate16 scenarios, each representing a distinct operating condition that reflects the combined stochastic behavior of sources and demand. These scenarios aim to replicate realistic fluctuations in power systems under uncertainty conditions. For each generated scenario, the corresponding joint probability (π_s) and the total active power loss (P_{loss}) were evaluated. The results presented in Figure 4.19, clearly illustrate the influence of combined wind and load uncertainties on system performance.

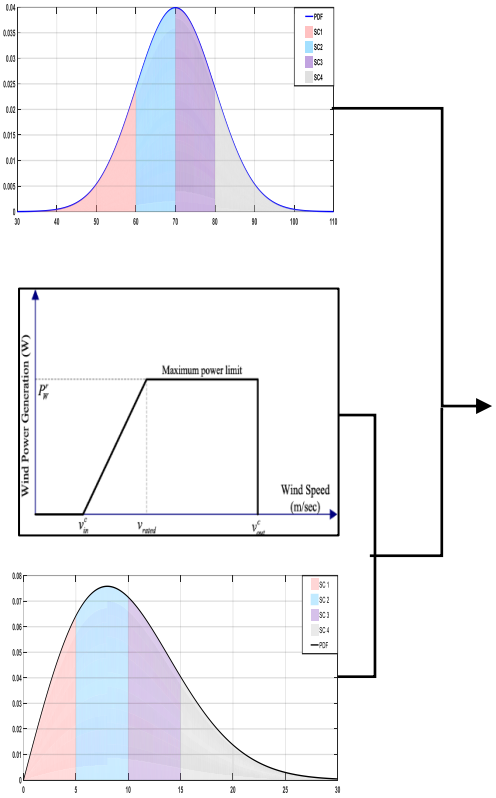

Scenario	Load %	Wind %	π_s	P_{loss}(MW)
Sc 1	54.754	10.893	0.0228	0.7102
Sc 2	54.754	25.13	0.0578	0.7905
Sc 3	54.754	40.89	0.0452	1.5367
Sc 4	54.754	61.533	0.0272	1.5199
Sc 5	65.401	10.893	0.0605	0.9475
Sc 6	65.401	25.13	0.1245	0.7609
Sc 7	65.401	40.89	0.0974	1.2383
Sc 8	65.401	61.533	0.0585	1.2419
Sc 9	74.599	10.893	0.0228	1.4583
Sc 10	74.599	25.13	0.0578	1.0395
Sc 11	74.599	40.89	0.0452	1.3014
Sc 12	74.599	61.533	0.0272	1.2896
Sc 13	85.246	10.893	0.0605	2.4103
Sc 14	85.246	25.13	0.1245	1.7412
Sc 15	85.246	40.89	0.0974	1.7126
Sc 16	85.246	61.533	0.0585	1.7056

Figure 4.19 : wind/load scenarios with their probabilities and active total losses.

Figure 4.19 shows The highest probability is observed in Scenarios 6 and 14, both with π_s = 0.1245, indicating they are the most likely operating conditions. Scenario 6 combines a moderate load (65.401%) with moderate wind (25.13%), resulting in a power loss of 0.7609 MW, while Scenario 14 reflects a high load (85.246%) and the same wind level (25.13%), leading to a higher loss of 1.7412 MW.

In contrast, the lowest probability is observed in Scenarios 1 and 9, both with π_s = 0.0228, and both representing low wind conditions (10.893%). Scenario 1, with the lowest load (54.754%), results in the lowest power loss of 0.7102 MW,and Scenario 9 with a higher load (74.599%), sees losses rise to 1.4583 MW.

These results highlight how both load and wind levels interact to influence system performance: low-probability scenarios may yield low losses but are rare, while high-

probability cases better reflect typical operation with moderate to high losses depending on demand.

- The simulation results by using the HO algorithm shows that all bus voltage magnitudes (Vm) stay within the allowed range, not passing the upper limit of 1.10 p.u, as seen in the voltage figure 4.20. In all 16 scenarios, no voltage problems were found, meaning the system keeps a stable voltage under different conditions .

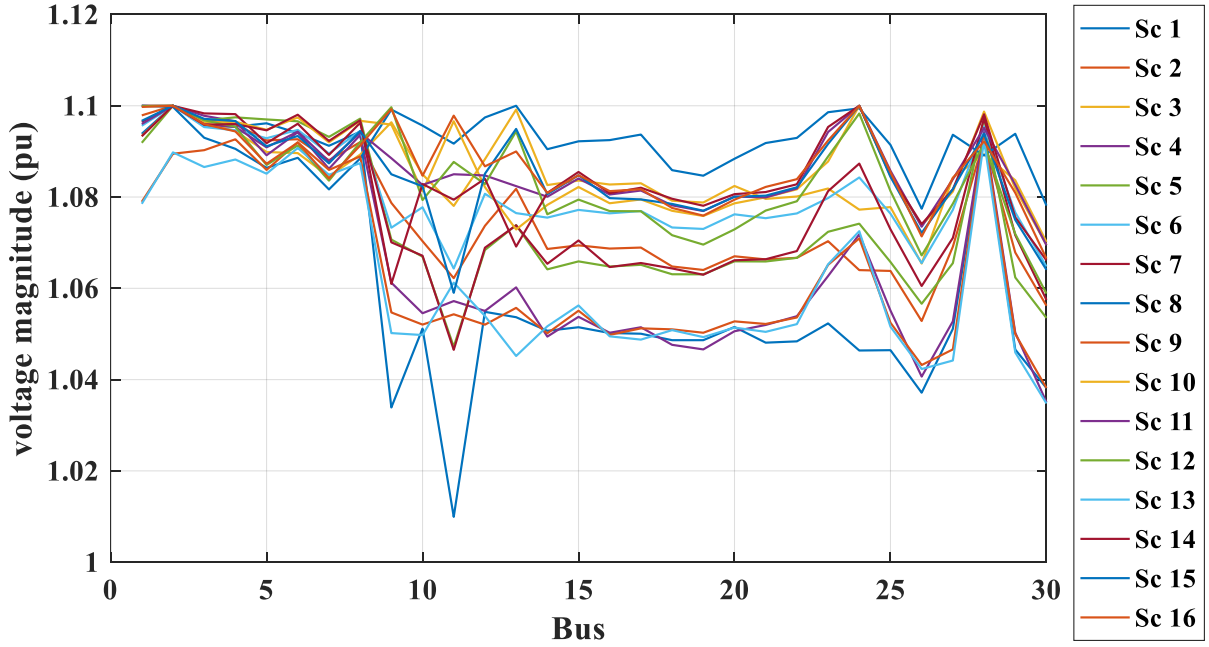

Figure 4.20 : Bus voltage magnitude profiles for IEEE 30-bus system under 16 wind/load scenarios.

- the generated reactive power (Qg) at all generator buses remains within the set minimum and maximum limits in table 4.12 and figure 4.21, The Qg shows that none of the scenarios caused these values to pass their allowed range. This proves that the proposed optimization HO method works well and keeps all control values safe and within limits, even with changes in wind and load.

Table 4. 12 : Reactive Power Generation (Qg) Scenarios with Minimum and Maximum lemittes.

	1	2	5	8	11	13	24
Qgmin	-20	-20	-15	-15	-10	-15	-15
Qgmax	200	100	80	60	50	60	9
Qg-Sc1	-6.3619	-3.9509	8.5153	13.3545	-9.2384	-0.6336	2.3493
Qg-Sc2	-5.8812	-3.7426	8.2787	13.6982	-9.4384	4.4332	2.6021

Qg-Sc3	-4.295	-3.6834	7.9699	9.1645	1.4311	-9.2087	1.3966
Qg-Sc4	-3.9628	-5.6927	8.1108	12.3432	-7.0747	0.0178	3.5043
Qg-Sc5	-6.7087	-5.9526	10.7795	14.4127	-8.0598	6.5072	3.0925
Qg-Sc6	-5.3248	-2.7404	10.4113	15.2725	11.0628	-3.0199	5.0953
Qg-Sc7	-5.335	-2.6649	11.1812	13.32	0.732	-6.8745	5.8569
Qg-Sc8	-5.2097	-2.5249	10.7266	12.4577	9.9375	-11.1056	2.0548
Qg-Sc9	-9.0222	-2.677	14.6408	19.051	-9.1513	8.7708	4.466
Qg-Sc10	-5.5668	-0.5655	13.3425	18.9625	-3.3037	-3.8263	3.8354
Qg-Sc11	-6.9307	-0.2648	13.6226	18.7387	-1.4798	-1.571	3.8159
Qg-Sc12	-5.9379	-1.9466	14.401	23.0807	-9.8625	7.9186	5.1455
Qg-Sc13	-9.6338	5.8312	17.1928	23.4169	2.0577	-2.34	5.5389
Qg-Sc14	-9.8839	4.3801	17.6402	23.3237	-3.5698	2.2514	5.2918
Qg-Sc15	-7.1332	-0.2954	16.9141	26.025	-5.9199	9.2601	8.0752
Qg-Sc16	-6.9748	0.1082	16.8476	21.8566	-0.4095	2.7744	4.6868

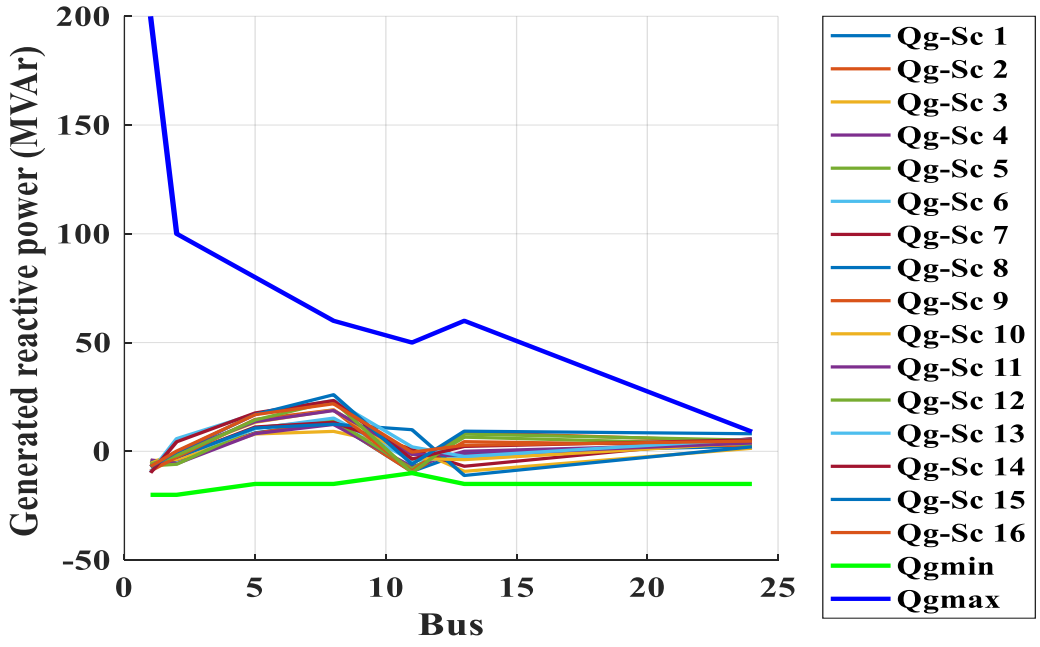

Figure 4.21 : Generated reactive power related to their minimum and maximum limits in the IEEE 30-bus test system under 16 wind/load scenarios.

4.7 Conclusion

The simulation results confirm that the Hippopotamus Optimization HO algorithm delivers high-quality and reliable solutions across a wide range of operating conditions. Whether under deterministic settings or various uncertainty scenarios including load, wind, and their combined effects the HO method consistently achieved effective minimization of active power losses, resulting in improved system efficiency.

In both the IEEE 30-bus and 57-bus systems, HO performed better than several other optimization methods, The HO algorithm showed faster convergence, lower losses, and enhanced voltage profiles. It also ensured that all voltage magnitudes stayed within acceptable bounds (≤1.10 p.u) and that reactive power generation remained within feasible limits across all generators.

In the presence of uncertainty, HO continued to demonstrate robust and stable performance. The Expected Power Loss (EPL) remained low in both wind and load scenarios, and even in the combined analysis, system security and control feasibility were preserved.

Overall, the results strongly validate the quality of the HO-based solution. The optimization was both technically effective and operationally secure, showing clear advantages in loss reduction, voltage regulation, and system stability under real-world variability.

General conclusion

General conclusion

This study is addressed to the Optimal Reactive Power Dispatch (ORPD) problem in modern power systems by incorporating both deterministic and probabilistic optimization frameworks. Initially, a comprehensive review of power flow theory and modeling of electrical components was provided to establish a solid foundation. Then, the Optimal reactive power dispatch problem was formulated under various objective functions, including power loss minimization, voltage deviation reduction, and voltage stability enhancement, while respecting physical and operational constraints.

To overcome the limitations of conventional methods, the Hippopotamus Optimization Algorithm HO has been proposeed as a recent bio-inspired metaheuristic based on the behavioral patterns of hippopotamuses. The algorithm's design combines exploration and exploitation strategies to improve convergence speed and solution accuracy.

Simulation results under deterministic condution on IEEE 30-bus and IEEE 57-bus systems demonstrated the effectiveness of HO compared to other well-known metaheuristic algorithms such as PSO, ABC, CLPSO, and SSA. The proposed method achieved better results in terms of minimizing active power losses, reducing voltage deviation, and improving voltage stability index.

Moreover, this study extended the analysis by considering uncertainty in both load demand and wind power generation using a probabilistic scenario-based approach. Incorporating these factors into optimization models leads to more realistic and reliable solutions that account for possible operational fluctuations. This, in turn, enhances the resilience and flexibility of the power grid, ensuring safe and continuous service delivery.

Based on these findings, the proposed approach can be considered a powerful tool for extending its application to OPF problem for large scale electric power systems. Future work may focus on expanding this approach to ORPD in larger-scale systems, integrating renewable energy sources, or developing more advanced hybrid models capable of handling uncertainties with greater accuracy.

References

References

[1] Pahwa, S., M. Youssef, and C. Scoglio. "Electrical networks: an introduction." Networks of networks: the last frontier of complexity (2014): 163-186.

[2] TRAN, Thomas TD et SMITH, Amanda D. "Thermoeconomic analysis of residential rooftop photovoltaic systems with integrated energy storage and resulting impacts on electrical distribution networks". Sustainable Energy Technologies and Assessments, 2018, vol. 29, p. 92-105.

[3] Abdellah, D." Répartition optimale des puissances utilisant les techniques de l'intelligence artificielle". Université des Frères Mentouri Constantine, Faculté des Sciences De l'Ingénieur, Département d'Electrotechnique, (2016).

[4] Hadji, B. "Contribution à l'Amélioration de l'Efficacité des Réseaux Electriques par l'Intégration et le Contrôle Flexible de l'Energie Eolienne et des Systèmes FACTS" (Doctoral dissertation, Université Mohamed Khider-Biskra), (2017).

[5] Hadi Saadat, « Power system analysis », McGraw-Hill series in electrical and computer enginnering, ISBN: 0-07-012235-0, (1999).

[6] Sekhane, H., & Labed, D. "Amélioration de l'ecoulement des puissances à travers les systèmes FACTS Pour les réseaux electriques" (Doctoral dissertation, Université Frères Mentouri-Constantine 1), (2019).

[7] Labed, D. & Bouzid, A." Production Décentralisée Et Couplage Au Réseau" [Thèse de Doctorat, Université Frères Mentouri - Constantine 1], (2008).

[8] MOUASSA, Souhil. "Optimisation de l'écoulement de puissance par une méthode métaheuristique (technique des abeilles) en présence d'une source renouvelable (éolienne) et des dispositifs FACTS". 2018. Thèse de doctorat.

[9] Mammeri, O. "Differentes methodes de calcul de la puissance reactive dans une noeud a charge non lineaire en presence d'un systeme de compensation de l'energie "(Doctoral dissertation, Université de Batna 2), (2012).

[10] . Guediri, A. "Application de la logique floue pour l'optimisation de l'écoulement de puissance" (Doctoral dissertation, Université Oum El Bouaghi),(2009).

[11] GRIGSBY, Leonard L. power systems . CRC press, 2007.

[12] VENKATASUBRAMANIAN, Mani. and Kevin Tomsovic. THE ELECTRICAL ENGINEERING HANDBOOK, 2004, p. 761.

[13] SYAH, Samir. "Application de l'intelligence artificielle pour le fonctionnement optimal des systèmes électrique". Thèse de doctorat. 2018.

[14] Chakraborty, K., & Chakrabarti, A. "Soft Computing Techniques in Voltage Security Analysis". Energy Systems in Electrical Engineering, (2015).

[15] SALHI, Souheil." Contribution to power flow optimization by enhanced artificial intelligence methods ". Doctoral dissertation. University Mohamed Khider Biskra, 2022.

[16] Murty, P. S. R. Load Flow Analysis. Electrical Power Systems, 527–587, (2017).

[17] Gómez-Expósito, Antonio, Antonio J. Conejo, and Claudio Cañizares, eds. Electric energy systems: analysis and operation. CRC press, 2018.

[18] M. YAHIAOUI, "Contrôle optimal des puissances réactives et des tensions dans un réseau d'énergie électrique par dispositifs FACTS," Thèse de Doctorat en Électrotechnique Option: Réseaux Electriques, 2014.

[19] AlRashidi, M. R., & El-Hawary, M. E. "Hybrid particle swarm optimization approach for solving the discrete OPF problem considering the valve loading effects". IEEE transactions on power systems, 22(4), 2030-2038, (2007).

[20] Reddy, P. L., & Yesuratnam, G." A modified bacterial foraging algorithm based optimal reactive power dispatch. Indonesian Journal of Electrical Engineering and Computer Science", 13(1), 361, (2019b).

[21] Basu, M. "Quasi-oppositional differential evolution for optimal reactive power dispatch. International journal of electrical power & energy systems", 78, 29-40, (2016).

[22] Mayouf, C., Salhi, A., Haidara, F., Aroua, F. Z., El-Sehiemy, R. A., Naimi, D., Aya, C., & Kane, C. S. E. "Solving optimal power flow using new efficient hybrid jellyfish search and moth flame optimization algorithms. Algorithms", 17(10), 438, (2024).

[23] CHAIB, Ala Eddine et MEHASNI, Rabia. "Étude de l'écoulement de puissance optimal par les méthodes d'optimisation Metaheuristiques". Thèse de doctorat. Université Frères Mentouri-Constantine 1, 2021.

[24] LE DINH, Luong, VO NGOC, Dieu, et VASANT, Pandian." Artificial bee colony algorithm for solving optimal power flow problem". The Scientific World Journal, 2013, vol. 2013, no 1, p. 159040.

[25] DUMAN, Serhat, GÜVENÇ, Uğur, SÖNMEZ, Yusuf, et al. "Optimal power flow using gravitational search algorithm. Energy conversion and management", 2012, vol. 59, p. 86-95.

[26] A. Schrijver. Theory of Linear and Integer Programming. Wiley, 1998.

[27] Nocedal, J., & Wright, S. J. (Eds.). Numerical optimization. New York, NY: Springer New York,(1999).

[28] Avriel, M .Nonlinear programming: analysis and methods. Courier Corporation,(2003).

[29] Mancer, N." Contribution à l'optimisation de la puissance réactive en présence de dispositif de compensation dynamique (FACTS)", (2012).

[30] G. Chen, L. Liu, Z. Zhang, and S. Huang, "Optimal reactive power dispatch by improved GSA-based algorithm with the novel strategies to handle constraints," Applied soft computing, vol. 50, pp. 58-70, 2017.

[31] Agbugba, E. "Hybridization of particle swarm optimization with bat algorithm for optimal reactive power dispatch". Diss. MSc Thesis, University of South Africa, 2017.

[32] Sharma, Tejaswini, et al. "Comparative study of methods for optimal reactive power dispatch." International Journal of Electrical and Electronics Engineering 3 (2014): 53-61.

[33] Mahadevan, K., and P. S. Kannan. "Comprehensive learning particle swarm optimization for reactive power dispatch." *Applied soft computing* 10.2 (2010): 641-652.

[34] Duman, Serhat, et al. "Optimal reactive power dispatch using a gravitational search algorithm." *IET generation, transmission & distribution* 6.6 (2012): 563-576.

[35] Ebeed, Mohamed, et al. "Solving the optimal reactive power dispatch using marine predators algorithm considering the uncertainties in load and wind-solar generation systems." Energies 13.17 (2020): 4316.

[36] Tabatabaei, Naser Mahdavi, et al., eds. "Reactive power control in AC power systems". Vol. 1. Springer International Publishing, 2017.

[37] Soroudi, A., & Amraee, T. "Decision making under uncertainty in energy systems: State of the art". Renewable and Sustainable Energy Reviews, 28, 376–384. (2013).

[38] Mohseni-Bonab, S. M., & Rabiee, A. "Optimal reactive power dispatch: a review, and a new stochastic voltage stability constrained multi-objective model at the presence of uncertain wind power generation". IET Generation, Transmission & Distribution, 11(4), 815-829, (2017).

[39] Mohseni-Bonab, S. M., Rabiee, A., & Mohammadi-Ivatloo, B. "Voltage stability constrained multi-objective optimal reactive power dispatch under load and wind power uncertainties: A stochastic approach. Renewable Energy", 85, 598-609, (2016).

[40] Biswas, Partha P., et al. "Optimal reactive power dispatch with uncertainties in load demand and renewable energy sources adopting scenario-based approach." Applied Soft Computing 75 (2019): 616-632.

[41] Amiri, Mohammad Hussein, et al. "Hippopotamus optimization algorithm: a novel nature-inspired optimization algorithm." *Scientific Reports* 14.1 (2024): 5032.

[42] HEIDARI, Ali Asghar, ABBASPOUR, Rahim Ali, et JORDEHI, Ahmad Rezaee. "Gaussian bare-bones water cycle algorithm for optimal reactive power dispatch in electrical power systems". Applied soft computing, 2017, vol. 57, p. 657-671.

[43] Aljohani, Tawfiq M., Ahmed F. Ebrahim, and Osama Mohammed. "Single and multiobjective optimal reactive power dispatch based on hybrid artificial physics–particle swarm optimization." *Energies* 12.12 (2019): 2333.